Chapter 16

Partially Coherent Beams

Overview: In this chapter we study the effects of a spatially partially coherent beam. Several investigations of the properties of such beams have led to the conclusion that the use of a diffuser at the exit aperture of a coherent laser can produce reduced scintillations at the receiver under the proper conditions. The same model, however, may also serve as a useful model for certain studies concerning the reflection of an optical wave from a partially rough surface.

We begin by reviewing the *Gaussian Schell-model* for the autocorrelation function of the surface roughness of the diffuser that is used in most studies of partially coherent beams. We then illustrate an equivalent formulation using the power spectral density for the diffuser roughness that we model as associated with a *thin phase screen.* The *mutual coherence function* for such a beam in free space is used to infer the spot size increase caused by the diffuser and the speckle size in both the receiver and detector plane. In developing models for the *scintillation index*, we take into account the coherence time of the detector versus that of the diffuser. In particular, we investigate the effect of a partially coherent beam in the presence of both slow and fast detectors. Also treated is the *bit error rate* (BER) for pulsed modulation using *on-off keying* (OOK) in a digital communication link operating in an open atmospheric channel.

The free-space analysis of an optical wave reflected from a *partially rough surface* such as that associated with certain lidar systems is explored through use of the same partially coherent beam model. By adjusting the surface roughness correlation length, such a target can take on characteristics associated with a smooth reflector (specular target) and also that of a fully diffuse or Lambertian target. Once again we consider separately slow and fast detectors with regard to the temporal fluctuations associated with the surface roughness.

16.1 Introduction

Studies of the propagation of a (spatially) *partially coherent beam wave* through atmospheric turbulence have been conducted over the past three decades by numerous researchers [1–24]. These studies include the case of scattering from a spatially rough target surface as well as those involving a partially coherent source. A partially coherent source can be generated in a number of different ways, including the placement of a diffuser at the exit aperture of a laser transmitter of a quasi-monochromatic source. The free-space second-order statistical characteristics of a partially coherent beam are discussed in detail in Mandel and Wolf [18] using a Gaussian Schell-model. Fourth-order statistics follow directly from second-order statistics only for the special case of a Gaussian-distributed field model.

Interest in the propagation of a partially coherent beam through atmospheric turbulence dates back to the work of Kon and Tatarskii [1] in the early 1970s. Theoretical foundations of partial coherence in free space were discussed much earlier but there was a lack of knowledge about the general behavior of such beams propagating through the atmosphere. During the 1970s and 1980s, expressions for the second- and fourth-order statistics of a partially coherent beam propagating through a random medium were developed for several special cases [3–13]. More recently there has been renewed interest in the notion of partial coherence and the possible use of transmitting a spatially partially coherent beam for improving the performance of a free-space optical (FSO) communication system [6–10].

Most studies concerning a spatially partially coherent beam wave rely on a Gaussian Schell-model for describing partial coherence of the source beam [18,19]. This permits one to express the spectral degree of coherence through the difference vector, $\mathbf{S} = \mathbf{s}_1 - \mathbf{s}_2$, where $\mathbf{s}_1$ and $\mathbf{s}_2$ are two points in the transmitter plane. Banakh et al. [10,20] showed that intensity fluctuations can decrease as the source spatial coherence decreases. In those studies, asymptotic results were derived for cases of both weak and strong intensity fluctuations. Fante [8] and Baykal et al. [11] considered the effects also of a temporally partially coherent source. In more recent studies [21–24], a model for a partially coherent source/target was developed from a phase screen facsimile for the diffuser/target that led to the implied scintillation index under general irradiance fluctuations.

The statistical properties of a partially coherent source, or light scattered by a rough target, have been studied from the points of view of either *temporal* or *spatial coherence*, assuming that the optical field obeys complex Gaussian statistics. When both temporal and spatial coherence effects are considered, the amplitude space-time correlation function of the Gaussian light is assumed to be factored into a product of temporal and spatial functions, i.e., the optical field satisfies the condition of *cross-spectral purity* [18].

16.2 Basic Beam Parameters

A schematic diagram for the propagation link involving a diffuser at the transmitter is shown in Fig. 16.1. We assume the transmitted wave is a TEM_{00} collimated Gaussian-beam wave that is characterized by beam parameters

$$\Theta_0 = 1, \quad \Lambda_0 = \frac{2L}{kW_0^2}, \tag{1}$$

where k is the optical wave number, W_0 is the beam radius at the $1/e$ point of the field, and L is propagation distance from the transmitter to the pupil plane of the receiver system. Ignoring the diffuser, the beam incident on the receiver lens has beam radius W_1 and phase front radius of curvature F_1 defined by the related beam parameters

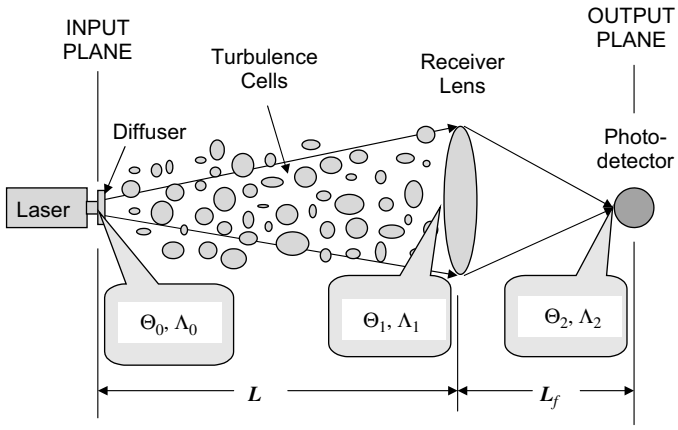

Figure 16.1 Propagation geometry and beam parameters with a diffuser at the exit aperture of a collimated beam.

$$\Theta_1 = \frac{\Theta_0}{\Theta_0^2 + \Lambda_0^2} = 1 + \frac{L}{F_1}, \quad \overline{\Theta}_1 = 1 - \Theta_1,$$
$$\Lambda_1 = \frac{\Lambda_0}{\Theta_0^2 + \Lambda_0^2} = \frac{2L}{kW_1^2}. \tag{2}$$

After passing through a receiver lens of "soft" aperture radius W_G and focal length F_G, the beam is characterized in the (image) plane of the detector by (see Chap. 10)

$$\Theta_2 = \frac{L}{L_f}\left[\frac{\dfrac{L}{L_f} - \dfrac{L}{F_G} + \overline{\Theta}_1}{\left(\dfrac{L}{L_f} - \dfrac{L}{F_G} + \overline{\Theta}_1\right)^2 + (\Lambda_1 + \Omega_G)^2}\right] = 0,$$
$$\Lambda_2 = \frac{L}{L_f}\left[\frac{\Lambda_1 + \Omega_G}{\left(\dfrac{L}{L_f} - \dfrac{L}{F_G} + \overline{\Theta}_1\right)^2 + (\Lambda_1 + \Omega_G)^2}\right] = \frac{L}{L_f(\Lambda_1 + \Omega_G)}, \tag{3}$$

where $\Omega_G = 2L/kW_G^2$ is a nondimensional parameter that depicts the finite size of the receiver lens. The beam radius W_2 in the image plane can be determined from Λ_2 through the relation

$$\Lambda_2 = \frac{2L_f}{kW_2^2}. \tag{4}$$

16.3 Mutual Coherence Function—Part I

The diffuser shown in Fig. 16.1 can be modeled by a Gaussian Schell-model (GSM) [19] or, equivalently, by a phase screen model [23] using a Gaussian spectrum (but not limited to this spectrum model) for the "strength" of the diffuser. In this section we discuss the GSM and introduce the phase screen model in Section 16.4.

16.3.1 Gaussian Schell-model

If a diffuser is placed at the exit aperture of a coherent laser transmitter, we can model the field of the optical wave emerging from the diffuser by

$$\tilde{U}_0(\mathbf{s},0) = U_0(\mathbf{s},0)\exp[i\varphi(\mathbf{s})], \tag{5}$$

where $U_0(\mathbf{s},0)$ is the field entering the diffuser, $\mathbf{s}$ is a transverse vector, and $\varphi(\mathbf{s})$ is a random phase with zero mean. In this setting we refer to $\tilde{U}_0(\mathbf{s},0)$ as the "effective source." In the GSM, it is customary to assume the correlation function associated with the random phase factor $\exp[i\varphi(\mathbf{s})]$ of the diffuser can be described by a Gaussian function, i.e.,

$$\begin{aligned} B(\mathbf{s}_1,\mathbf{s}_2,0) &= \langle \tilde{U}_0(\mathbf{s}_1,0)\tilde{U}_0^*(\mathbf{s}_2,0)\rangle \\ &= U_0(\mathbf{s}_1,0)U_0^*(\mathbf{s}_2,0)\langle \exp\{i[\varphi(\mathbf{s}_1)-\varphi(\mathbf{s}_2)]\}\rangle \\ &= U_0(\mathbf{s}_1,0)U_0^*(\mathbf{s}_2,0)\exp\left(-\frac{|\mathbf{s}_1-\mathbf{s}_2|^2}{2\sigma_c^2}\right), \end{aligned} \tag{6}$$

where σ_c^2 is a measure of the *correlation width* of the diffuser that describes the partial coherence properties of the effective transmitted source. For example, if $\sigma_c^2 \gg 1$, the source is essentially a coherent wave, whereas if σ_c^2 is comparable in size with the wavelength of the laser source, the effective transmitted source acts like an incoherent wave (strong diffuser case). In some studies, the coherence properties of the source are described by the *source coherence parameter* [16–18]

$$\zeta_s = 1 + \frac{W_0^2}{\sigma_c^2}, \tag{7}$$

which we can interpret to represent the number of "speckle cells" (i.e., statistically independent patches) at the diffuser. For a weak diffuser ($\sigma_c^2 \gg W_0^2$), the number of speckle cells is one (a coherent wave), but many speckle cells will normally exist for the case of a strong diffuser. Each speckle cell acts like an independent source term.

16.3.2 Free-space analysis in the pupil plane

By using the extended Huygens-Fresnel principle (Chaps. 5 and 7), the MCF at the pupil plane (pp) of the receiver for a quasi-monochromatic Gaussian laser source is defined by

$$\Gamma_{\text{pp, diff}}(\mathbf{r}_1, \mathbf{r}_2, L) = \frac{k^2}{4\pi^2 L^2} \int\int_{-\infty}^{\infty} d^2 s_1 \int\int_{-\infty}^{\infty} d^2 s_2 \langle \tilde{U}_0(\mathbf{s}_1, 0) \tilde{U}_0^*(\mathbf{s}_2, 0) \rangle \times \exp\left[\frac{ik}{2L} |\mathbf{s}_1 - \mathbf{r}_1|^2 - \frac{ik}{2L} |\mathbf{s}_2 - \mathbf{r}_2|^2 \right], \tag{8}$$

which, using the correlation function (6), reduces to

$$\Gamma_{\text{pp, diff}}(\mathbf{r}_1, \mathbf{r}_2, L) = \frac{k^2}{4\pi^2 L^2} \int\int_{-\infty}^{\infty} d^2 s_1 \int\int_{-\infty}^{\infty} d^2 s_2 \exp\left(-\frac{s_1^2 + s_2^2}{W_0^2} \right) \exp\left(-\frac{|\mathbf{s}_1 - \mathbf{s}_2|^2}{l_c^2} \right) \times \exp\left[\frac{ik}{2L} |\mathbf{s}_1 - \mathbf{r}_1|^2 - \frac{ik}{2L} |\mathbf{s}_2 - \mathbf{r}_2|^2 \right], \tag{9}$$

where we now introduce the *correlation radius* $l_c = \sqrt{2}\sigma_c$. In arriving at (9), we have assumed the transmitted wave is a collimated beam with unit amplitude. The evaluation of the integrals in (9) then leads to

$$\Gamma_{\text{pp, diff}}(\mathbf{r}_1, \mathbf{r}_2, L) = \frac{W_0^2}{W_1^2(1 + 4\Lambda_1 q_c)} \exp\left[\frac{ik}{L} \left(\frac{1 - \Theta_1 + 4\Lambda_1 q_c}{1 + 4\Lambda_1 q_c} \right) \mathbf{r} \cdot \mathbf{p} \right] \times \exp\left[-\frac{2r^2 + \rho^2/2}{W_1^2(1 + 4\Lambda_1 q_c)} \right] \exp\left[-\left(\frac{\Theta_1^2 + \Lambda_1^2}{1 + 4\Lambda_1 q_c} \right) \left(\frac{\rho^2}{l_c^2} \right) \right], \tag{10}$$

where $\mathbf{p} = \mathbf{r}_1 - \mathbf{r}_2, \rho = |\mathbf{p}|$, and $\mathbf{r} = (1/2)(\mathbf{r}_1 + \mathbf{r}_2)$. The quantity W_1 is the spot size radius in the pupil plane for a completely coherent source and q_c is a nondimensional coherence parameter defined by

$$q_c = \frac{L}{k l_c^2}. \tag{11}$$

All second-order statistics can be determined from the general expression (10). For example, by setting $\mathbf{r}_1 = \mathbf{r}_2 = \mathbf{r}$ we find that the *mean irradiance* in the pupil plane is

$$\langle I(\mathbf{r}, L) \rangle_{\text{pp, diff}} = \frac{W_0^2}{W_1^2(1 + 4\Lambda_1 q_c)} \exp\left[-\frac{2r^2}{W_1^2(1 + 4\Lambda_1 q_c)} \right], \tag{12}$$

where we can interpret the spot size radius due to a partially coherent beam by the expression

$$W_{\text{pp, diff}} = W_1 \sqrt{1 + 4\Lambda_1 q_c}. \tag{13}$$

Similarly, by considering the normalized MCF, we obtain the *modulus of the complex degree of coherence* (DOC)

$$\text{DOC}_{\text{pp, diff}}(\rho, L) = \frac{|\Gamma_{\text{pp, diff}}(\mathbf{r}_1, \mathbf{r}_2, L)|}{\sqrt{\Gamma_{\text{pp, diff}}(\mathbf{r}_1, \mathbf{r}_1, L) \Gamma_{\text{pp, diff}}(\mathbf{r}_2, \mathbf{r}_2, L)}} = \exp\left[-\left(\frac{\Theta_1^2 + \Lambda_1^2}{1 + 4\Lambda_1 q_c} \right) \frac{\rho^2}{l_c^2} \right], \tag{14}$$

from which we deduce the *mean speckle radius*

$$\rho_{\text{pp, speckle}} = \sqrt{\frac{l_c^2(1+4\Lambda_1 q_c)}{\Theta_1^2+\Lambda_1^2}} = \frac{l_c}{W_0} W_{\text{pp, diff}}. \tag{15}$$

Note that this last result implies that the number of speckle cells at the source remains in constant ratio between input and output planes, i.e.,

$$\frac{W_0^2}{l_c^2} = \frac{W_{\text{pp, diff}}^2}{\rho_{\text{pp, speckle}}^2}. \tag{16}$$

Also, in the limit of a strong diffuser ($l_c \to 0$), the average speckle radius becomes

$$\rho_{\text{pp, speckle}} = \frac{2\sqrt{2}L}{kW_0} = \frac{\sqrt{2}\lambda L}{\pi W_0}. \tag{17}$$

16.4 Mutual Coherence Function—Part II

In this section we first develop the mutual coherence function (MCF) from a random phase screen model in the absence of atmospheric effects. We will develop expressions valid for both the pupil plane of the receiver and the image plane. Although in our analysis we only use the Gaussian power spectrum for describing the spatial fluctuations of the random phase screen, other spectral models for the random phase screen can easily be introduced in this approach. However, the Gaussian spectrum model is featured because it leads to results identical with those produced by more conventional methods based on the GSM. Last, we also discuss the MCF in the presence of atmospheric effects.

16.4.1 Random phase screen model

Here we model the diffuser at the exit aperture of the laser transmitter by a thin random phase screen (see Chap. 15) that induces a complex phase perturbation on the transmitted wave at the source. However, we will characterize the phase screen by its spatial power spectrum rather than by its correlation function as in the GSM. If we assume the diffuser is completely described by a single scale size associated with the correlation radius of the diffuser, we can use a single scale spectrum model. To be consistent with results deduced from the GSM, we will assume a *Gaussian spectrum*

$$\Phi_S(\kappa) = \frac{\langle n_1^2\rangle l_c^3}{8\pi\sqrt{\pi}} \exp\left(-\frac{l_c^2\kappa^2}{4}\right), \tag{18}$$

where l_c is the *lateral correlation radius* directly related to the parameter σ_c^2 of the GSM by $l_c^2 = 2\sigma_c^2$, and the parameter $\langle n_1^2\rangle$ describes the index of refraction fluctuations associated with the phase screen. Clearly, a Gaussian spectrum is equivalent to the assumption of a Gaussian correlation function used in the

GSM (e.g., see Problem 1). To compare results based on this formulation of the diffuser with those based on the GSM, we use the power spectrum (18) combined with conventional Rytov theory as presented in Chap. 15. Also, we will henceforth use only the parameter l_c for the diffuser correlation radius.

16.4.2 Free-space analysis in the pupil plane

If the optical wave at the transmitter is a unit-amplitude collimated beam characterized by beam parameters (1), then the field in the pupil plane of the receiver can be represented by

$$U(\mathbf{r}, L) = U_0(\mathbf{r}, L) \exp[\Psi_S(\mathbf{r}, L)], \tag{19}$$

where $\Psi_s(\mathbf{r}, L)$ is the complex phase perturbation caused by the diffuser (phase screen). By using the results of Eqs. (16)–(18) in Chap. 15 with $d_3 = 1$ (i.e., the phase screen is placed at the source), it follows that the MCF in this case is defined by

$$\begin{aligned}\Gamma_{\text{pp, diff}}(\mathbf{r}_1, \mathbf{r}_2, L) = \Gamma_0(\mathbf{r}_1, \mathbf{r}_2, L) \exp\Bigg\{ &-4\pi^2 k^2 \Delta z \int_0^\infty \kappa \Phi_S(\kappa) \\ &\times \left[1 - e^{-\Lambda_1 L \kappa^2/k} J_0(\kappa|\Theta_1 \mathbf{p} - 2i\Lambda_1 \mathbf{r}|)\right] d\kappa \Bigg\},\end{aligned} \tag{20}$$

where Δz is the thickness of the phase screen and $\Gamma_0(\mathbf{r}_1, \mathbf{r}_2, L)$ is the MCF in the absence of the diffuser defined by

$$\Gamma_0(\mathbf{r}_1, \mathbf{r}_2, L) = \frac{W_0^2}{W_1^2} \exp\left(-\frac{2r^2}{W_1^2} - \frac{\rho^2}{2W_1^2} - i\frac{k}{F_1}\mathbf{p} \cdot \mathbf{r}\right). \tag{21}$$

By rearranging terms according to Eq. (36) in Chap. 6, we have

$$\begin{aligned}\Gamma_{\text{pp, diff}}(\mathbf{r}_1, \mathbf{r}_2, L) = \Gamma_0(\mathbf{r}_1, \mathbf{r}_2, L) &\exp\left[\sigma^2_{r,\,\text{diff}}(\mathbf{r}_1, L) + \sigma^2_{r,\,\text{diff}}(\mathbf{r}_2, L)\right] \\ &\times \exp[-T_{\text{diff}}(L)] \exp\left[-\frac{1}{2}\Delta_{\text{diff}}(\mathbf{r}_1, \mathbf{r}_2, L)\right],\end{aligned} \tag{22}$$

where each radial term $\sigma^2_{r,\,\text{diff}}(\mathbf{r}, L)$ is linked to a change in the mean irradiance profile, $T_{\text{diff}}(L)$ describes the longitudinal or on-axis change in mean irradiance, and $\text{Re}[\Delta_{\text{diff}}(\mathbf{r}_1, \mathbf{r}_2, L)] = D_{\text{diff}}(\mathbf{r}_1, \mathbf{r}_2, L)$ is the wave structure function (WSF).

Based on the Gaussian spectrum (18), each radial component in (22) reduces to

$$\begin{aligned}\sigma^2_{r,\,\text{diff}}(\mathbf{r}, L) &= 2\pi^2 k^2 \Delta z \int_0^\infty \kappa \Phi_S(\kappa) e^{-\Lambda_1 L \kappa^2/k} [I_0(2\Lambda_1 r\kappa) - 1] d\kappa \\ &= \frac{\sqrt{\pi}\langle n_1^2 \rangle k^2 l_c \Delta z}{2(1 + 4\Lambda_1 q_c)} \left\{ \exp\left[\frac{4\Lambda_1^2 r^2}{(1 + 4\Lambda_1 q_c) l_c^2}\right] - 1 \right\}.\end{aligned} \tag{23}$$

To equate these results with those based on the GSM, we introduce the

normalization

$$\frac{\sqrt{\pi}\langle n_1^2\rangle k^2 l_c \Delta z}{1+4\Lambda_1 q_c} = 1, \tag{24}$$

and then use the small argument approximation for the exponential function consistent with Rytov theory to obtain

$$\sigma_{r,\,\mathrm{diff}}^2(\mathbf{r}, L) = \frac{2\Lambda_1^2 r^2}{(1+4\Lambda_1 q_c) l_c^2} = \frac{4\Lambda_1 q_c}{1+4\Lambda_1 q_c}\left(\frac{r^2}{W_1^2}\right). \tag{25}$$

Similarly, the longitudinal component in (22) leads to

$$T_{\mathrm{diff}}(L) = 4\pi^2 k^2 \Delta z \int_0^\infty \kappa \Phi_S(\kappa)\left(1 - e^{-\Lambda_1 L\kappa^2/k}\right) d\kappa = 4\Lambda_1 q_c, \tag{26}$$

where we have again used the normalization (24) and the small argument approximation. The remaining quantity in (22) can be obtained directly from the result of (25) and replacing $\mathbf{r}_1 = \mathbf{r} - \mathbf{p}/2, \mathbf{r}_2 = \mathbf{r} + \mathbf{p}/2,$ which yields

$$\begin{aligned}\Delta_{\mathrm{diff}}^2(\mathbf{r}_1, \mathbf{r}_2, L) &= 4\pi^2 k^2 \Delta z \int_0^\infty \kappa \Phi_S(\kappa) e^{-\Lambda_1 L\kappa^2/k} \\ &\quad \times [I_0(2\Lambda_1 r_1 \kappa) + I_0(2\Lambda_1 r_2 \kappa) - 2J_0(\kappa|\Theta_1 \mathbf{p} - 2i\Lambda_1 \mathbf{r}|)] d\kappa \\ &= 2\left(\frac{\Theta_1^2 + \Lambda_1^2}{1+4\Lambda_1 q_c}\right)\frac{\rho^2}{l_c^2} - \frac{4i\Theta_1 \mathbf{p}\cdot\mathbf{r}}{(1+4\Lambda_1 q_c) l_c^2}.\end{aligned} \tag{27}$$

Last, by combining the results of (25) through (27), we arrive at

$$\begin{aligned}\Gamma_{\mathrm{pp,\,diff}}(\mathbf{r}_1, \mathbf{r}_2, L) &= \frac{W_0^2}{W_1^2(1+4\Lambda_1 q_c)} \exp\left[\frac{ik}{L}\left(\frac{1-\Theta_1+4\Lambda_1 q_c}{1+4\Lambda_1 q_c}\right)\mathbf{r}\cdot\mathbf{p}\right] \\ &\quad \times \exp\left[-\frac{2r^2 + \rho^2/2}{W_1^2(1+4\Lambda_1 q_c)}\right] \exp\left[-\left(\frac{\Theta_1^2+\Lambda_1^2}{1+4\Lambda_1 q_c}\right)\left(\frac{\rho^2}{l_c^2}\right)\right],\end{aligned} \tag{28}$$

where we have also used the approximation $\exp[-T_{\mathrm{diff}}(L)] \cong 1/[1 + T_{\mathrm{diff}}(L)]$. We recognize (28) as the same result obtained from the GSM [see Eq. (10)]. Consequently, the beam spot radius and speckle radius deduced from the phase screen model are both exactly the same as those obtained in Section 16.3.2.

16.4.3 Free-space analysis in the image plane

For the image plane (ip) analysis we first calculate the *ABCD* matrix for the entire propagation path (minus the diffuser) shown in Fig. 16.1, viz.,

$$\begin{aligned}\begin{pmatrix} A & B \\ C & D \end{pmatrix} &= \begin{pmatrix} 1 & L_f \\ 0 & 1 \end{pmatrix}\begin{pmatrix} 1 & 0 \\ i\alpha_G & 1 \end{pmatrix}\begin{pmatrix} 1 & L \\ 0 & 1 \end{pmatrix} \\ &= \begin{pmatrix} 1+i\alpha_G L_f & L+L_f(1+i\alpha_G L) \\ i\alpha_G & 1+i\alpha_G L \end{pmatrix},\end{aligned} \tag{29}$$

where $\alpha_G = 2/kW_G^2 + i/F_G$. The free-space optical field in the image plane is then given by the generalized Huygens-Fresnel integral (see Chap. 10), which leads to

$$U_0(\mathbf{r}, L+L_f) = \frac{1}{A+i\alpha_0 B}\exp\left[ik(L+L_f) - \frac{1}{2}\left(\frac{\alpha_0 D - iC}{A+i\alpha_0 B}\right)kr^2\right], \tag{30}$$

where (for a collimated beam)

$$\alpha_0 = \frac{2}{kW_0^2}. \tag{31}$$

Although we could use the GSM for developing the MCF in the image plane, we do so only for the simpler phase screen model, which yields

$$\begin{aligned}\Gamma_{\text{ip,diff}}(\mathbf{r}_1, \mathbf{r}_2, L+L_f) = \Gamma_0(\mathbf{r}_1, \mathbf{r}_2, L+L_f)\exp\left[\sigma^2_{r,\text{diff}}(\mathbf{r}_1, L+L_f) + \sigma^2_{r,\text{diff}}(\mathbf{r}_2, L+L_f)\right] \\ \times \exp\left[-T_{\text{diff}}(L+L_f)\right]\exp\left[-\frac{1}{2}\Delta_{\text{diff}}(\mathbf{r}_1, \mathbf{r}_2, L+L_f)\right],\end{aligned} \tag{32}$$

where the first term on the right-hand side is now given by

$$\Gamma_0(\mathbf{r}_1, \mathbf{r}_2, L+L_f) = \frac{W_0^2}{W_2^2}\exp\left(-\frac{2r^2}{W_2^2} - \frac{\rho^2}{2W_2^2} - i\frac{k}{F_2}\mathbf{p}\cdot\mathbf{r}\right). \tag{33}$$

Each radial component in (32) takes the form

$$\begin{aligned}&\sigma^2_{r,\text{diff}}(\mathbf{r}, L+L_f) \\ &= 2\pi^2 k^2 \Delta z \int_0^\infty \kappa\Phi_S(\kappa)\exp\left[-\frac{(\Theta_1^2 + \Lambda_1\Omega_G)L\kappa^2}{k(\Lambda_1+\Omega_G)}\right]\left\{I_0\left[\frac{2L\Theta_1 r\kappa}{L_f(\Lambda_1+\Omega_G)}\right] - 1\right\}d\kappa \\ &= \frac{\sqrt{\pi}\langle n_1^2\rangle k^2 l_c \Delta z}{1 + 4q_c\left(\frac{\Theta_1^2+\Lambda_1\Omega_G}{\Lambda_1+\Omega_G}\right)}\left\{\exp\left[\frac{4L^2\Theta_1^2 r^2/l_c^2 L_f^2}{(\Lambda_1+\Omega_G+4q_c(\Theta_1^2+\Lambda_1\Omega_G)}\right] - 1\right\}.\end{aligned} \tag{34}$$

Here, the normalization (24) is replaced by the slightly more general expression

$$\frac{\sqrt{\pi}\langle n_1^2\rangle k^2 l_c \Delta z}{1+4q_c\left(\dfrac{\Theta_1^2+\Lambda_1\Omega_G}{\Lambda_1+\Omega_G}\right)}=1, \tag{35}$$

and, by invoking the small argument approximation for the last exponential function in (34), we find that (34) reduces to

$$\sigma_{r,\mathrm{diff}}^2(\mathbf{r},L+L_f)=\frac{2L^2\Theta_1^2 r^2}{l_c^2 L_f^2(\Lambda_1+\Omega_G)\left[1+4q_c\left(\dfrac{\Theta_1^2+\Lambda_1\Omega_G}{\Lambda_1+\Omega_G}\right)\right]}. \tag{36}$$

In a similar manner, the longitudinal component in (32) leads to

$$T_{\mathrm{diff}}(L+L_f)=4q_c\left(\frac{\Theta_1^2+\Lambda_1\Omega_G}{\Lambda_1+\Omega_G}\right). \tag{37}$$

From these expressions we deduce that the mean irradiance in the image plane can be approximated by the Gaussian function

$$\langle I(\mathbf{r},L+L_f)\rangle_{\mathrm{ip,diff}}=\frac{W_0^2}{W_{\mathrm{ip,diff}}^2}\exp\left(-\frac{2r^2}{W_{\mathrm{ip,diff}}^2}\right), \tag{38}$$

where the image plane spot radius is

$$W_{\mathrm{ip,\ diff}}=W_2\sqrt{1+4q_c\left(\frac{\Theta_1^2+\Lambda_1\Omega_G}{\Lambda_1+\Omega_G}\right)}. \tag{39}$$

In the absence of the diffuser, the image plane spot radius is defined by use of Eq. (4), but can be well approximated by the expression $W_2\cong\lambda F_G/\pi W_G, L\gg L_f$.

Following an analysis similar to that given in Section 16.4.2 for the pupil plane, here we find that the modulus of the complex degree of coherence in the image plane becomes

$$\mathrm{DOC}_{\mathrm{ip,diff}}(\rho,L)=\exp\left\{-\left[\frac{\Theta_1^2+\Lambda_1^2}{(\Lambda_1+\Omega_G)\left[\Lambda_1+\Omega_G+4q_c(\Theta_1^2+\Lambda_1\Omega_G)\right]}\right]\frac{L^2\rho^2}{L_f^2 l_c^2}\right\}, \tag{40}$$

from which we deduce the mean speckle size

$$\begin{aligned}\rho_{\mathrm{ip,speckle}}&=\frac{L_f l_c}{L}\sqrt{\frac{(\Lambda_1+\Omega_G)\left[\Lambda_1+\Omega_G+4q_c(\Theta_1^2+\Lambda_1\Omega_G)\right]}{\Theta_1^2+\Lambda_1^2}}\\&=\left(\frac{l_c}{W_0}\right)\left(\frac{W_1}{W_G}\right)W_{\mathrm{ip,diff}}.\end{aligned} \tag{41}$$

Note that by comparing (41) with the pupil plane expression (15), we can write the image plane speckle radius as the ratio

$$\frac{\rho_{\text{ip, speckle}}}{\rho_{\text{pp, speckle}}} = \left(\frac{W_1}{W_G}\right)\left(\frac{W_{\text{ip, diff}}}{W_{\text{pp, diff}}}\right). \tag{42}$$

In the limiting case of a strong diffuser ($l_c \to 0$), we see that (42) becomes

$$\frac{\rho_{\text{ip, speckle}}}{\rho_{\text{pp, speckle}}} = \left(\frac{W_2}{W_G}\right)\sqrt{\frac{\Theta_1^2 + \Lambda_1\Omega_G}{\Lambda_1(\Lambda_1 + \Omega_G)}}, \qquad l_c \to 0. \tag{43}$$

For the case of a small receiver lens ($\Omega_G \gg 1$), the square-root factor reduces to unity and we see that the ratio (43) is simply the ratio of image plane spot radius to lens radius, which is the same result as that for a coherent source and any size lens.

16.4.4 Atmospheric effects in the pupil plane

In the presence of atmospheric turbulence, the field of the optical wave in the pupil plane of the receiver is modeled by

$$U(\mathbf{r}, L) = U_0(\mathbf{r}, L)\exp[\Psi_S(\mathbf{r}, L)]\exp[\psi_1(\mathbf{r}, L) + \psi_2(\mathbf{r}, L)], \tag{44}$$

where $\psi_1(\mathbf{r}, L)$ and $\psi_2(\mathbf{r}, L)$ represent first-order and second-order complex phase perturbations due to atmospheric turbulence and $\Psi_s(\mathbf{r}, L)$ is the complex phase perturbation induced by the diffuser. We will assume that the complex phase perturbations caused by the diffuser and those by the atmosphere are *statistically independent.* Under this assumption the MCF in the pupil plane can be written in the factored form

$$\Gamma_2(\mathbf{r}_1, \mathbf{r}_2, L) = \Gamma_{\text{pp, diff}}(\mathbf{r}_1, \mathbf{r}_2, L)\Gamma_{\text{atm}}(\mathbf{r}_1, \mathbf{r}_2, L), \tag{45}$$

where the first factor is that given by (28) above and the second factor, caused by atmospheric effects on a coherent source, is given by (36) in Chap. 6. For the special case in which $\mathbf{r}_2 = -\mathbf{r}_1$ and a Kolmogorov power-law spectrum

$$\Phi_n(\kappa) = 0.033C_n^2\kappa^{-11/3}, \tag{46}$$

where C_n^2 is the refractive-index structure parameter, the modulus of the MCF due to atmospheric effects alone can be expressed as (see Section 6.4.2)

$$|\Gamma_{\text{atm}}(\mathbf{r}_1, -\mathbf{r}_1, L)| = \exp\left[2\sigma_{r,\text{atm}}^2(\rho/2, L) - T_{\text{atm}}(L)\right]\exp\left[-\left(\frac{\rho}{\rho_0}\right)^{5/3}\right], \tag{47}$$

where

$$\rho_0 = \left[\frac{8}{3(a + 0.62\Lambda^{11/6})}\right]^{3/5} (1.46C_n^2 k^2 L)^{-3/5}, \quad l_0 \ll \rho_0 \ll L_0, \tag{48}$$

$$a = \begin{cases} \dfrac{1 - \Theta^{8/3}}{1 - \Theta}, & \Theta \geq 0 \\ \dfrac{1 + |\Theta|^{8/3}}{1 - \Theta}, & \Theta < 0, \end{cases} \tag{49}$$

$$\sigma^2_{r,\,\mathrm{atm}}(\rho/2, L) = 1.11\sigma_R^2 \Lambda_1^{5/6} \frac{\rho^2}{4W_1^2}, \quad \rho < 2W_1, \tag{50}$$

$$T_{\mathrm{atm}}(L) = 1.33\sigma_R^2 \Lambda_1^{5/6}. \tag{51}$$

The quantity $\sigma_R^2 = 1.23C_n^2 k^{7/6} L^{11/6}$, called the *Rytov variance*, is a measure of the strength of irradiance fluctuations, which in the present discussion we assume is less than unity corresponding to the regime of weak irradiance fluctuations.

The mean irradiance in the pupil plane due to the combined effects of the diffuser and atmospheric turbulence is readily obtained from the MCF by setting $\mathbf{r}_1 = \mathbf{r}_2 = \mathbf{r}$, and is given by the Gaussian approximation

$$\langle I(\mathbf{r}, L)\rangle = \frac{W_0^2}{W_{\mathrm{eff}}^2} \exp\left(-\frac{2r^2}{W_{\mathrm{eff}}^2}\right), \tag{52}$$

where the effective (long-term) spot radius is

$$W_{\mathrm{eff}} = W_1 \sqrt{1 + 4\Lambda_1 q_c + 1.33\sigma_R^2 \Lambda_1^{5/6}}. \tag{53}$$

Thus, both atmospheric turbulence and the diffuser cause spreading of the beam beyond that due to diffraction alone. However, for the case of a strong diffuser in which $q_c \gg \sigma_R^2$, the spreading of the optical wave is caused primarily by the diffuser rather than by atmospheric turbulence.

Under the influence of atmospheric effects and the diffuser, the modulus of the complex degree of coherence deduced from the MCF (45) leads to

$$\mathrm{DOC}(\rho, L) = \exp\left[-\left(\frac{\Theta_1^2 + \Lambda_1^2}{1 + 4\Lambda_1 q_c}\right)\frac{\rho^2}{l_c^2} + \left(\frac{\rho}{\rho_0}\right)^{5/3}\right]. \tag{54}$$

To estimate the spatial coherence radius implied by the $1/e$ point of (54), we use the approximation $(\rho/\rho_0)^{5/3} \cong (\rho/\rho_0)^2$, from which we obtain

$$\rho_{0,\,\mathrm{eff}} = \left[\frac{\Theta_1^2 + \Lambda_1^2}{l_c^2(1 + 4\Lambda_1 q_c)} + \frac{1}{\rho_0^2}\right]^{-1/2}, \tag{55}$$

or, in terms of the beam radius (13),

$$\rho_{0,\,\mathrm{eff}} = \frac{\rho_0}{\sqrt{1 + \left(\dfrac{W_0}{l_c}\right)^2 \left(\dfrac{\rho_0}{W_{\mathrm{pp,\,diff}}}\right)^2}}. \tag{56}$$

Belen'kii and Mironov [4] developed a similar expression for the spatial coherence radius of a partially coherent source using the extended Huygens-Fresnel principle and a quadratic approximation for the WSF. In fact, numerical results from (55) [or (56)] differ very little from those deduced from the expression in Ref. [4] under weak irradiance fluctuations.

16.5 Scintillation Index—Part I

In this and the next section we calculate the *scintillation index* caused by the combination of diffuser and atmospheric turbulence under weak and general irradiance fluctuations. In making scintillation calculations with a diffuser at the source, it is the integrated irradiance that we must consider, taking into account the coherence time τ_S of the source and the response time τ_D of the detector. The *coherence time* of a quasi-monochromatic laser source is defined by $\tau_S \cong 1/B$, where B is the bandwidth of the source. If the source coherence time is much smaller than the detector's integration time interval, i.e., if $\tau_S \ll \tau_D$, we have what is called a "slow detector" and temporal averaging of the fluctuating irradiance occurs. This temporal averaging reduces the scintillation level through "source aperture averaging" [8,10]. In the case of a "fast detector," i.e., $\tau_S \gg \tau_D$, the detector is sensitive to irradiance fluctuations of the source as well as those caused by the atmospheric turbulence. In both cases above, the coherence time τ_{atm} of the atmospheric turbulence is slow with respect to τ_S and τ_D.

In this section we limit our discussion to the slow detector case ($\tau_S \ll \tau_D \ll \tau_{\mathrm{atm}}$) and in Section 16.6 consider the case of a fast detector ($\tau_D \ll \tau_S \ll \tau_{\mathrm{atm}}$). In each case the impact of using a partially coherent beam on a free-space optics (FSO) link is studied through development of the implied bit error rate (BER).

16.5.1 Longitudinal component

Because we are taking the case of a slow detector, the scintillation index induced by the diffuser alone in the absence of atmospheric turbulence is taken to be essentially zero. In the presence of atmospheric effects, we need to take into account some scattering properties caused by the diffuser. Namely, each scattering center (speckle cell size) associated with the spatial correlation radius l_c of the diffuser surface acts like a separate beam coherence center within the original beam source diameter. Hence, the diffuser creates an "array of independent scattering centers," the number of which can be approximated by [see also Eq. (7)]

$$N_S = 1 + \frac{2W_0^2}{l_c^2} = 1 + \frac{4q_c}{\Lambda_0}. \tag{57}$$

To account for this behavior of the beam emerging from the diffuser, we find it useful to model the beam at the pupil plane of a receiver by an "effective diffuser beam" that changes in accordance with the correlation radius l_c of the diffuser in relation to the coherent beam radius W_0. We can characterize the effective diffuser (*ed*) beam at the receiver by replacing the standard beam parameters Θ_1 and Λ_1 with a set of effective beam parameters Θ_{ed} and Λ_{ed}. These effective beam parameters are identified by simply comparing parameters of the MCF in the absence of the diffuser with parameters associated with the MCF in the presence of the diffuser. For example, the MCF (21) at the pupil plane in the absence of the diffuser and scaled by the on-axis irradiance can be written as

$$\frac{\Gamma_0(\mathbf{r},\mathbf{p},L)}{\Gamma_0(0,0,L)} = \exp\left(-\frac{\Lambda_1 k r^2}{L} - \frac{\Lambda_1 k \rho^2}{4L} + \frac{ik\overline{\Theta}_1}{L}\mathbf{p}\cdot\mathbf{r}\right). \tag{58}$$

Similarly, from Eq. (28) we obtain the scaled MCF in the presence of a diffuser

$$\frac{\Gamma_{\mathrm{pp,\,diff}}(\mathbf{r},\mathbf{p},L)}{\Gamma_{\mathrm{pp,\,diff}}(0,0,L)} = \exp\left[-\frac{\Lambda_1 k r^2}{(1+4\Lambda_1 q_c)L} - \frac{\Lambda_1 N_S k \rho^2}{4(1+4\Lambda_1 q_c)L} + \frac{ik(\overline{\Theta}_1 + 4\Lambda_1 q_c)}{(1+4\Lambda_1 q_c)L}\mathbf{p}\cdot\mathbf{r}\right]. \tag{59}$$

Upon comparing similar terms appearing in (58) and (59), the effective radius of curvature of the beam can be identified in (59) by the last term involving the complex argument, viz.,

$$\overline{\Theta}_{ed} = -\frac{L}{F_{ed}} = \frac{\overline{\Theta}_1 + 4\Lambda_1 q_c}{1+4\Lambda_1 q_c}. \tag{60}$$

For a weak diffuser, we find that $\overline{\Theta}_{ed} = \overline{\Theta}_1$ (i.e., the phase front radius of curvature F_{ed} reduces to its free-space value F_1 in the absence of the diffuser). Hence, we can introduce the complementary beam parameter

$$\Theta_{ed} = 1 - \overline{\Theta}_{ed} = \frac{\Theta_1}{1+4\Lambda_1 q_c} = \frac{\Theta_0}{\Theta_0^2 + \Lambda_0^2 N_S}, \tag{61}$$

where we have related Θ_{ed} to the transmitter plane parameters in the last step, which also involves the number of speckle cells (57).

In defining the effective beam parameter Λ_{ed} we are faced with a different situation. Namely, the term involving ρ^2 in (59) can be associated with longitudinal characteristics of the beam wave induced by the diffuser (rather than specific points in the beam). On the other hand, the term involving r^2 in (59) can be identified with the radial characteristics of the beam such as beam size and beam wander. Because we are concerned here only with the longitudinal behavior of the scintillation index, we will use the ρ^2 term in (59) to identify the effective beam parameter

$$\Lambda_{ed} = \frac{\Lambda_1 N_S}{1+4\Lambda_1 q_c} = \frac{\Lambda_0 N_S}{\Theta_0^2 + \Lambda_0^2 N_S}, \tag{62}$$

limiting cases of which lead to

$$\Lambda_{ed} = \begin{cases} \Lambda_1, & q_c \to 0 \\ 1/\Lambda_0, & q_c \to \infty. \end{cases} \tag{63}$$

It is behavior depicted by the lower expression in (63) that we find contributes to transmitter aperture averaging for a strong diffuser. We take note of the fact that the equivalent parameter found in the r^2 term in (59) is the same as (62), but for the case in which $N_S = 1$ in the numerator.

Based on the above observations, the longitudinal component of the scintillation index for a beam characterized by beam parameters (61) and (62) is that given by Eq. (14) in Chap. 8, but with the conventional beam parameters formally replaced by (61) and (62). This action leads to the result

$$\sigma^2_{I,\mathrm{atm}}(0,L) \equiv \sigma^2_{B,\mathrm{diff}} = 3.86\sigma_R^2 \mathrm{Re}\left[i^{5/6}\, {}_2F_1\left(-\frac{5}{6},\, \frac{11}{6};\, \frac{17}{6};\, \overline{\Theta}_{ed} + i\Lambda_{ed} \right) - \frac{11}{16}\Lambda_{ed}^{5/6} \right]. \tag{64}$$

We plot Eq. (64) in Fig. 16.2 as a function of propagation distance L and various correlation radii l_c for the diffuser, including the implied scintillation index for a coherent source. The assumed wavelength is $\lambda = 1.55\mu$m, the beam diameter is 5 cm, and we took a refractive index structure parameter value $C_n^2 = 5 \times 10^{-14}\mathrm{m}^{-2/3}$. Here we see that source aperture averaging becomes quite significant whenever the number of speckle cells from the diffuser becomes large. In the figure, this happens for a diffuser correlation radius of $l_c \leq 0.01$ m, corresponding to 13+ speckle cells.

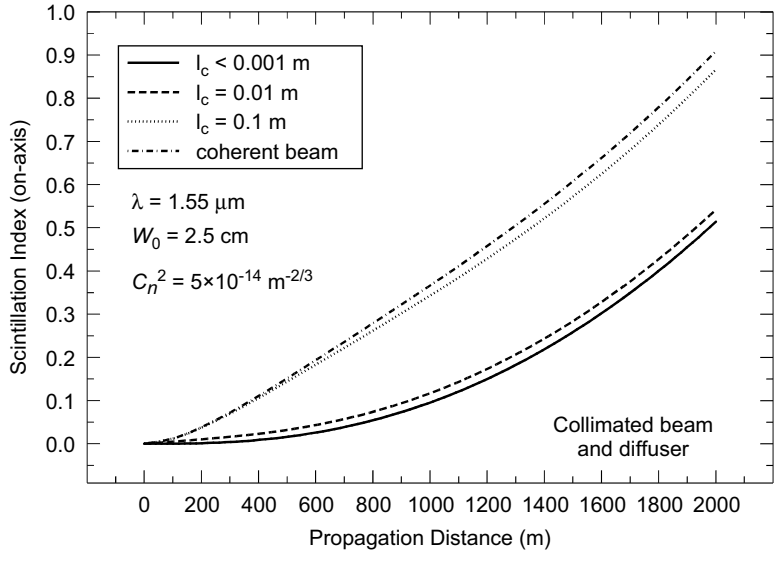

Figure 16.2 Effective scintillation index (on-axis) of a partially coherent beam under weak irradiance fluctuations as a function of propagation distance.

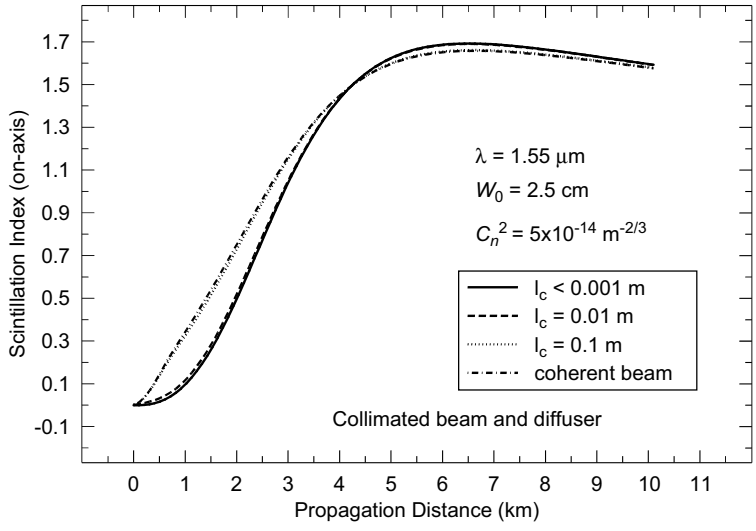

Figure 16.3 Same as Fig. 16.2 except the propagation distance is permitted to extend into strong irradiance fluctuations.

Equation (64) is restricted to weak irradiance fluctuations. If we use the strong fluctuation theory from Chap. 9 [see Eq. (101) in Chap. 9], then we have

$$\sigma_{I,\mathrm{atm}}^2(0,L) = \exp\left\{\frac{0.49\sigma_{B,\mathrm{diff}}^2}{\left[1+0.56(1+\Theta_{ed})\sigma_{B,\mathrm{diff}}^{12/5}\right]^{7/6}} + \frac{0.51\sigma_{B,\mathrm{diff}}^2}{\left(1+0.69\sigma_{B,\mathrm{diff}}^{12/5}\right)^{5/6}}\right\} - 1, \tag{65}$$

where $\sigma_{B,\mathrm{diff}}^2$ is that defined by (64). As discussed in Chap. 9, this expression is valid under all fluctuation conditions, but neglects any effects from inner and outer scale.

In Fig. 16.3 we plot Eq. (65) for longer propagation distances L but other conditions the same as cited for Fig. 16.2. In this case, however, we see that there is a propagation distance at which the partially coherent beam does not lower scintillation, but in fact leads to greater values because the beam appears more and more spherical due to diffuser-induced beam spreading. In Fig. 16.3 this happens in the vicinity of 4 km, suggesting that source aperture averaging is most effective over shorter ranges. For other wavelengths, beam size, and refractive index structure parameter, the results will be somewhat different, but there will exist some maximum propagation distance at which source aperture averaging fails to lower scintillation.

16.5.2 Radial component

At a point in the receiver pupil plane off the optical axis, the scintillation index can be expressed as the sum of two components (see Chaps. 8 and 9)

$$\sigma_{I,\mathrm{atm}}^2(\mathbf{r},L) = \sigma_{I,r,\mathrm{atm}}^2(\mathbf{r},L) + \sigma_{I,\mathrm{atm}}^2(0,L), \tag{66}$$

where the first component is called the radial component and the second component is the longitudinal component discussed in Section 16.5.1. The radial component vanishes on the optical axis ($r = 0$) and, under weak irradiance fluctuations with no diffuser, is given by

$$\sigma_{I,r}^2(\mathbf{r}, L) = 4.42\sigma_R^2 \Lambda_1^{5/6} \frac{r^2}{W_1^2}, \qquad r < W_1,\ \sigma_R^2 < 1. \tag{67}$$

By following the approach used in Chap. 9 for extending (67) into the strong fluctuation regime, we will formally replace the parameters in (67) with the effective parameters

$$\begin{aligned} W_1 &\Rightarrow W_1\sqrt{1 + 4\Lambda_1 q_c + 1.63\sigma_R^{12/5}\Lambda_1}, \\ \Lambda_1 &\Rightarrow \frac{2L}{kW_1^2(1 + 4\Lambda_1 q_c + 1.63\sigma_R^{12/5}\Lambda_1)} = \frac{\Lambda_1}{1 + 4\Lambda_1 q_c + 1.63\sigma_R^{12/5}\Lambda_1}. \end{aligned} \tag{68}$$

This action, which also accounts for the diffuser, leads to the expression

$$\begin{aligned} \sigma_{I,r,\mathrm{atm}}^2(\mathbf{r}, L) = 4.42\sigma_R^2 &\left(\frac{\Lambda_1}{1 + 4\Lambda_1 q_c + 1.63\sigma_R^{12/5}\Lambda_1}\right)^{5/6} \\ &\times \frac{r^2}{W_1^2(1 + 4\Lambda_1 q_c + 1.63\sigma_R^{12/5}\Lambda_1)}, \qquad r < W_1, \end{aligned} \tag{69}$$

which is now assumed to be valid under both weak and strong irradiance fluctuations. In both (67) and (69) we have imposed the constraint $r < W_1$, although this may be more restrictive than necessary. The full range of validity for these expressions has not yet been established. In the limit $\sigma_R^2 \to \infty$, Eq. (69) predicts that the radial component vanishes as the beam acts more and more like a propagating spherical wave. The same result occurs in the case of a sufficiently strong diffuser (i.e., $q_c \to \infty$). In this latter case, the source is essentially that of an incoherent optical wave.

In Fig. 16.4 we show the radial component (69) as a function of radial distance off the optical axis scaled by the spot radius at the receiver. All conditions are similar to those in Figs. 16.2 and 16.3 except here we replace the case $l_c = 0.1$ m with $l_c = 0.05$ m and have fixed the propagation distance at 1 km. Note that the radial component is essentially eliminated by a strong diffuser.

16.6 Scintillation Index—Part II

In this section we consider the implied scintillation index for arbitrary ratios of the coherence time of the source τ_S and the response time of the detector τ_D. To begin, however, we will consider the fast detector case in the absence of atmospheric turbulence.

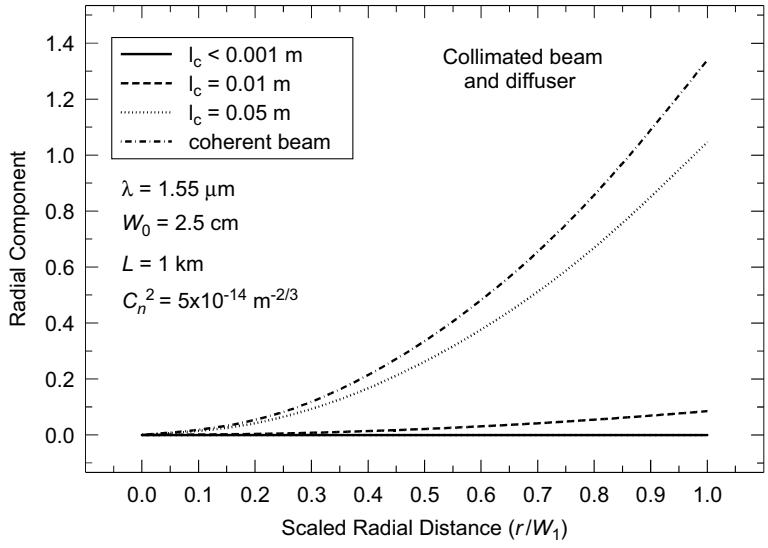

Figure 16.4 Radial component of the scintillation index as a function of radial distance scaled by the free-space spot radius.

16.6.1 Fast detector case: free space

If the response time of the detector is much shorter than the coherence time of the source (i.e., if $\tau_D \ll \tau_S$), the detector will be sensitive to irradiance fluctuations of the source. In this case the phase screen model (in the absence of atmospheric effects) leads to [24]

$$\sigma_{I,\mathrm{diff}}^2(0,L) = 8\pi^2 k^2 \Delta z \int_0^\infty \kappa \Phi_S(\kappa) e^{-\Lambda_1 L\kappa^2/k} \left[1 - \cos\left(\frac{\Theta_1 L\kappa^2}{k}\right)\right] d\kappa, \tag{70}$$

which, by use of the Gaussian spectrum (18), yields

$$\sigma_{I,\mathrm{diff}}^2(0,L) = 1 - \frac{1 + 4\Lambda_1 q_c}{(1 + 4\Lambda_1 q_c)^2 + 16\Theta_1^2 q_c^2}. \tag{71}$$

In deriving (71), we have used the normalization

$$\frac{2\sqrt{\pi}\langle n_1^2\rangle k^2 l_c \Delta z}{1 + 4\Lambda_1 q_c} = 1. \tag{72}$$

Limiting cases of (71) are $\sigma_{I,\mathrm{diff}}^2(0,L) = 0$ for a weak diffuser ($l_c \to \infty$) and $\sigma_{I,\mathrm{diff}}^2(0,L) = 1$ for a strong diffuser ($l_c \to 0$). The strong diffuser case corresponds to a spatially incoherent beam.

16.6.2 Integrated intensity

The integrated irradiance (intensity) can be represented by

$$E(\mathbf{r}, \mathbf{L}) = \frac{1}{T}\int_{-T/2}^{T/2} I(\mathbf{r}, L; t)dt, \tag{73}$$

where $I(\mathbf{r}, L; t)$ is the instantaneous irradiance and T is the integration time. From linear system analysis, we recognize (73) as the output of an ideal integrator with the impulse response function

$$h(t) = \frac{1}{T}U(T - |t|),$$

where $U(t)$ is the unit step function. The corresponding system function is therefore

$$\frac{\sin \omega T/2}{\omega T/2},$$

which is the Fourier transform of the impulse response function $h(t)$. It follows that the (on-axis) variance of the integrated intensity (73) is related to the covariance function of the input by [25,26]

$$\sigma^2_{I,E}(0, L) = \sigma^2_{I,\text{diff}}(0, L)\left[\frac{1}{T}\int_{-T}^{T}\left(1 - \frac{|\tau|}{T}\right)|\gamma(\tau)|^2 d\tau\right], \tag{74}$$

where $|\gamma(\tau)|^2$ is the normalized temporal covariance function of the instantaneous source irradiance. In arriving at (74), we have divided by the square of the mean irradiance to obtain the scintillation index (normalized variance) and we have assumed the covariance function of the input can be expressed as a product of the spatial covariance and temporal covariance. It is interesting that the above integral yields similar numerical values for several models of $|\gamma(\tau)|^2$; e.g., (74) produces roughly the same results for either a Gaussian or Lorentzian spectrum [25]. If we use a Lorentzian spectrum model, for example, it follows that $\gamma(\tau) = e^{-|\tau|/\tau_s}$, and in this case we can replace the time period T in (74) with the response time of the detector τ_D. The result of doing so yields the expression

$$\sigma^2_{I,E}(0, L) = \sigma^2_{I,\text{diff}}(0, L)\left[\frac{\tau_S}{\tau_D} + \frac{1}{2}\left(\frac{\tau_S}{\tau_D}\right)^2\left(e^{-2\tau_D/\tau_S} - 1\right)\right]. \tag{75}$$

Equation (75) gives us the scintillation index of the integrated intensity as an arbitrary function of coherence time of the source and response time of the detector. The two limiting cases of a fast detector and slow detector are readily deduced from (75), which leads to

$$\sigma^2_{I,E}(0, L) = \begin{cases} \sigma^2_{I,\text{diff}}(0, L), & \tau_D \ll \tau_S \\ \dfrac{\tau_S}{\tau_D}\sigma^2_{I,\text{diff}}(0, L), & \tau_D \gg \tau_S. \end{cases} \tag{76}$$

In the lower case (slow detector case) the ratio τ_S/τ_D approaches zero, which eliminates all irradiance fluctuations associated with the diffuser alone.

16.6.3 Longitudinal component

We assume the instantaneous (normalized) irradiance for a "point aperture" receiver can be expressed as the product $I = EI_{\text{atm}}$, where E is the on-axis integrated irradiance of the source and I_{atm} is the random on-axis irradiance due to atmosphere and diffuser. If we further assume that these components are statistically independent, then

$$\begin{aligned} \langle I(0,L)\rangle &= \langle E(0,L)\rangle\langle I_{\text{atm}}(0,L)\rangle = 1, \\ \langle I^2(0,L)\rangle &= \langle E^2(0,L)\rangle\langle I^2_{\text{atm}}(0,L)\rangle = \big[1+\sigma^2_{I,E}(0,L)\big]\big[1+\sigma^2_{I,\text{atm}}(0,L)\big], \end{aligned} \tag{77}$$

where $\sigma^2_{I,E}(0,L)$ is defined by (75) and $\sigma^2_{I,\text{atm}}(0,L)$ is the "slow detector" expression given by (65). In this case, the scintillation index takes the form

$$\sigma_I^2(0,L) = \frac{\langle I^2(0,L)\rangle}{\langle I(0,L)\rangle^2} - 1 = \sigma^2_{I,\text{atm}}(0,L) + \sigma^2_{I,E}(0,L)\big[1+\sigma^2_{I,\text{atm}}(0,L)\big]. \tag{78}$$

Note that in the limit of a strong diffuser and fast detector, this last result becomes

$$\sigma_I^2(0,L) = 1 + 2\sigma^2_{I,\text{atm}}(0,L), \qquad l_c \to 0, \ \frac{\tau_S}{\tau_D} \gg 1. \tag{79}$$

In Figs. 16.5–16.7 we display the scintillation index (78) under different irradiance fluctuation conditions corresponding to weak, moderate, and strong

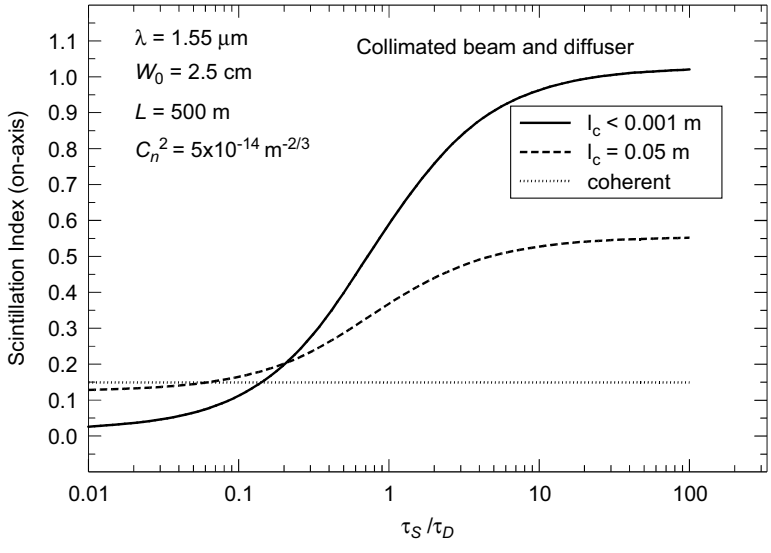

Figure 16.5 Scintillation index vs. relative detector speed in weak irradiance fluctuations ($\sigma_R^2 = 0.28$).

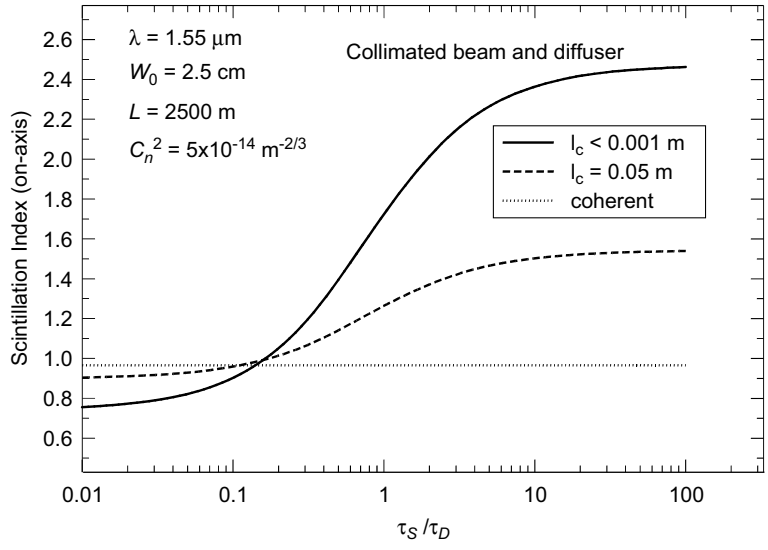

Figure 16.6 Scintillation index vs. relative detector speed in moderate irradiance fluctuations ($\sigma_R^2 = 5.3$).

fluctuations. In all cases we take a collimated beam of diameter 5 cm, wavelength 1.55 μm, and various values of the ratio τ_S/τ_D. Along every curve there is a value of the ratio τ_S/τ_D at which the diffuser leads to a larger scintillation value than that of a coherent wave. It is interesting that under moderate irradiance fluctuations (Fig. 16.6), this ratio is a little higher than it is in weak fluctuations. Under sufficiently strong irradiance fluctuations (Fig. 16.7), there is little to no improvement

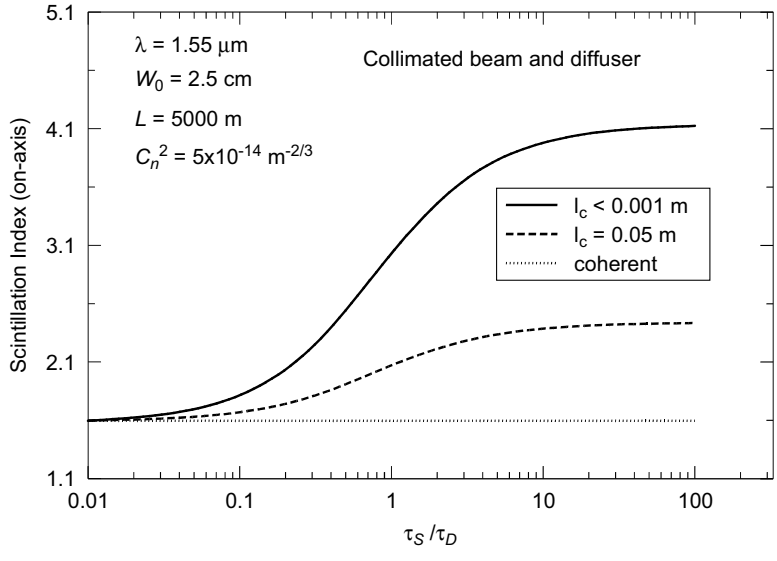

Figure 16.7 Scintillation index vs. relative detector speed in strong irradiance fluctuations ($\sigma_R^2 = 19$).

in reducing scintillation under any ratio τ_S/τ_D. Clearly, the slow-detector case ($\tau_S/\tau_D \ll 1$) leads to the greatest reduction of scintillation in the presence of a diffuser.

16.7 FSO Communication Systems

In Chaps. 11 and 12 we provided an analysis of the deleterious effects of scintillation for various FSO communication system channels using a coherent optical wave. In particular, in Chap. 11 we examined the benefit of using a large-aperture receiver system, or a multiple-aperture receiver array, on a terrestrial FSO link for reducing scintillation [and hence produce less signal fade and lower bit error rate (BER)] through aperture averaging.

In this section we wish to further examine FSO system performance based on the use of a (spatially) partially coherent wave. However, the reduction in the on-axis scintillation index due to partial coherence of the source, as discussed in Section 16.6, is not sufficient by itself for high quality data transfer in terms of BER for most FSO communication systems. A receiver system with a partially coherent source may allow for the use of a smaller size receiver aperture and still provide the necessary BER for a specified system performance level.

16.7.1 Scintillation model in the image plane

In Section 16.4 we presented a free-space analysis of the MCF in both the pupil plane and the image plane of the receiver. Here we wish to develop a scintillation model for a partially coherent beam that is valid in the image plane of the receiver system.

Referring to Section 10.3.5, the irradiance flux variance at the image plane in the limiting case $l_0 = 0$ and $L_0 = \infty$ can be expressed as

$$\sigma_I^2(\Omega_G) = \exp\left[\sigma_{\ln X}^2(L + L_f, \Omega_G) + \sigma_{\ln Y}^2(L + L_f, \Omega_G)\right] - 1, \qquad \Omega_G \geq \Lambda_1, \quad (80)$$

where the large-scale and small-scale log variances are

$$\sigma_{\ln X}^2(L+L_f,\Omega_G) = \frac{0.49\left(\dfrac{\Omega_G - \Lambda_{ed}}{\Omega_G + \Lambda_{ed}}\right)^2 \sigma_{B,\text{diff}}^2}{\left[1 + \dfrac{0.4(2-\overline{\Theta}_{ed})(\sigma_{B,\text{diff}}/\sigma_R)^{12/7}}{(\Omega_G + \Lambda_{ed})\left(\dfrac{1}{3} - \dfrac{1}{2}\overline{\Theta}_{ed} + \dfrac{1}{5}\overline{\Theta}_{ed}^2\right)^{6/7}} + 0.56\sigma_{B,\text{diff}}^{12/5}\right]^{7/6}}, \quad (81)$$

$$\sigma_{\ln Y}^2(L+L_f,\Omega_G) = \frac{\dfrac{0.51\sigma_{B,\text{diff}}^2}{\left(1 + 0.69\sigma_{B,\text{diff}}^{12/5}\right)^{5/6}}}{1 + \dfrac{1.20(\sigma_R/\sigma_{B,\text{diff}})^{12/5} + 0.83\sigma_R^{12/5}}{\Omega_G + \Lambda_{ed}}}, \quad (82)$$

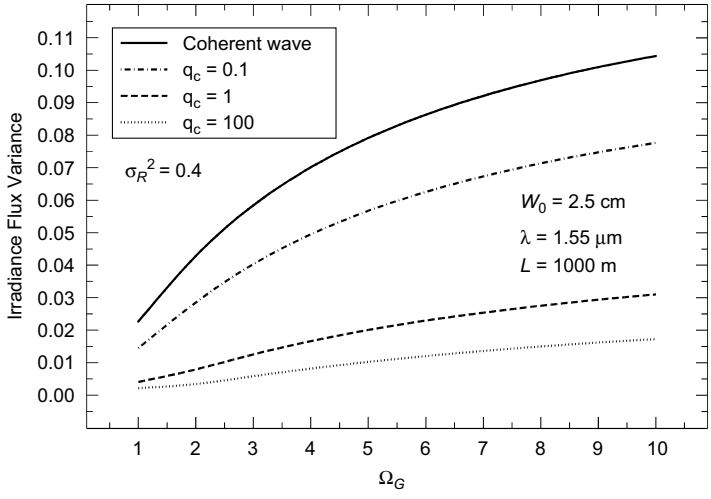

Figure 16.8 Irradiance flux variance in the image plane of a receiver system as a function of partial coherence q_c and normalized receiver aperture size Ω_G. Atmospheric conditions lead to weak irradiance fluctuations in the pupil plane.

and the Rytov variance for a Gaussian beam wave is given by

$$\sigma_{B,\mathrm{diff}}^2 = 3.86\sigma_R^2 \mathrm{Re}\left[i^{5/6} {}_2F_1\left(-\frac{5}{6}, \frac{11}{6}; \frac{17}{6}; \overline{\Theta}_{ed} + i\Lambda_{ed} \right) - \frac{11}{16}\Lambda_{ed}^{5/6} \right]. \tag{83}$$

In Figs. 16.8–16.10 we illustrate the irradiance flux variance as a function of normalized receiver aperture size $\Omega_G = 2L/kW_G^2$, where W_G is the receiver

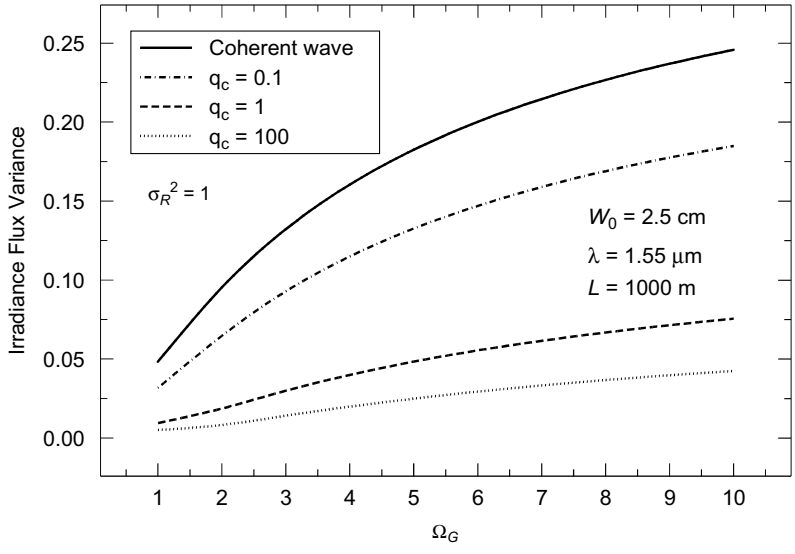

Figure 16.9 Same as Fig. 16.8 for moderate irradiance fluctuations in the pupil plane.

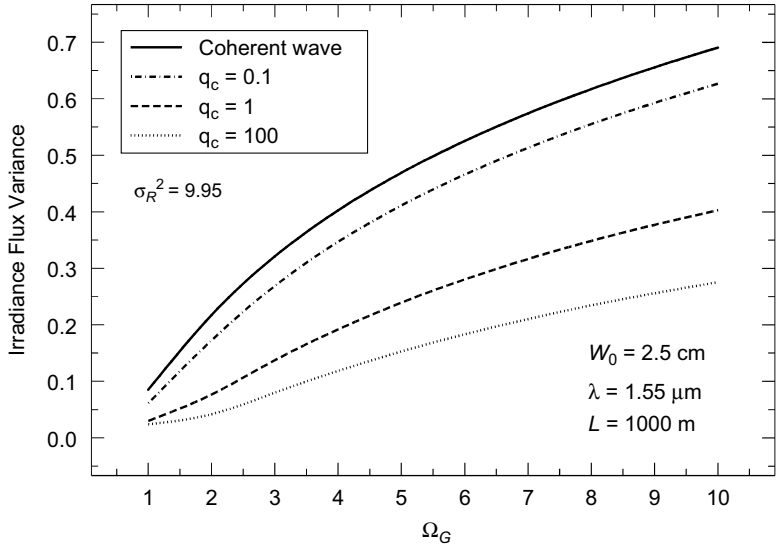

Figure 16.10 Same as Fig. 16.8 for strong irradiance fluctuations in the pupil plane.

radius. In each figure we assume the transmitted beam radius is $W_0 = 2.5\,\text{cm}$, the wavelength is $\lambda = 1.55\,\mu\text{m}$, and the path length is 1 km. For such beams we then compare the predicted irradiance flux variance in the image plane of a partially coherent beam ($q_c = L/kl_c^2 = 0.1,\ 1,\ 100$) with that of a spatially coherent beam at the transmitter. The case $q_c = 100$ is essentially the same as that for an incoherent beam. Figure 16.8 characterizes the regime of weak irradiance fluctuations with $\sigma_R^2 = 0.4$, Fig. 16.9 illustrates the onset of the focusing regime with $\sigma_R^2 = 1$, and Fig. 16.10 represents strong irradiance fluctuations with $\sigma_R^2 = 9.95$. The greatest reduction in the irradiance flux variance for a partially coherent beam occurs in the weak fluctuation regime (Fig. 16.8).

16.7.2 Bit error-rate (BER) performance

Following Section 11.4.3, the *probability of error*, or BER, is defined by the expression

$$\Pr(E) = \langle \text{BER} \rangle = \frac{1}{2}\int_0^\infty p_I(u)\text{erfc}\left(\frac{\langle \text{SNR} \rangle u}{2\sqrt{2}}\right) du, \tag{84}$$

where we will assume that $p_I(u)$ is the *gamma-gamma distribution* with unit mean

$$p_I(u) = \frac{2(\alpha\beta)^{(\alpha+\beta)/2}}{\Gamma(\alpha)\Gamma(\beta)} u^{(\alpha+\beta)/2-1} K_{\alpha-\beta}\left(2\sqrt{\alpha\beta u}\right), \qquad u > 0. \tag{85}$$

The quantity $\langle \text{SNR} \rangle$ is the mean signal-to-noise ratio (SNR) and the parameters of the gamma-gamma PDF model are defined by

$$\alpha = \frac{1}{\exp\left[\sigma^2_{\ln X}(L + L_f, \Omega_G\right] - 1}, \quad \beta = \frac{1}{\exp\left[\sigma^2_{\ln Y}(L + L_f, \Omega_G\right] - 1}. \tag{86}$$

In Figs. 16.11 and 16.12 we plot the mean BER obtained through numerical integration of (84) as a function of $\langle \text{SNR} \rangle$ in decibels (dB). In Fig. 16.11 we use the same beam and atmospheric characteristics as those leading to Fig. 16.8 under weak irradiance fluctuations, whereas in Fig. 16.12 we use the beam parameters and atmospheric conditions identified in Fig. 16.9 that correspond to the onset of moderate-to-strong irradiance fluctuations. To emphasize the improvement of using a partially coherent beam over the improvement due to aperture averaging alone, we choose a receiver aperture of diameter 2 cm and a roughness correlation length of the diffuser $l_c = 1$ cm. For contrast, we also show in both figures the probability of error for a coherent beam at the transmitter and that in free space, the latter in the absence of atmospheric effects. Clearly, under these conditions the use of a partially coherent beam can improve the mean BER by a significant amount, particularly under weak-to-moderate irradiance fluctuations. Under strong irradiance fluctuations ($\sigma_R^2 \gg 1$) we have found the effectiveness of using a partially coherent beam begins to diminish and aperture averaging alone (with larger apertures) may lead to better system performance [23,24].

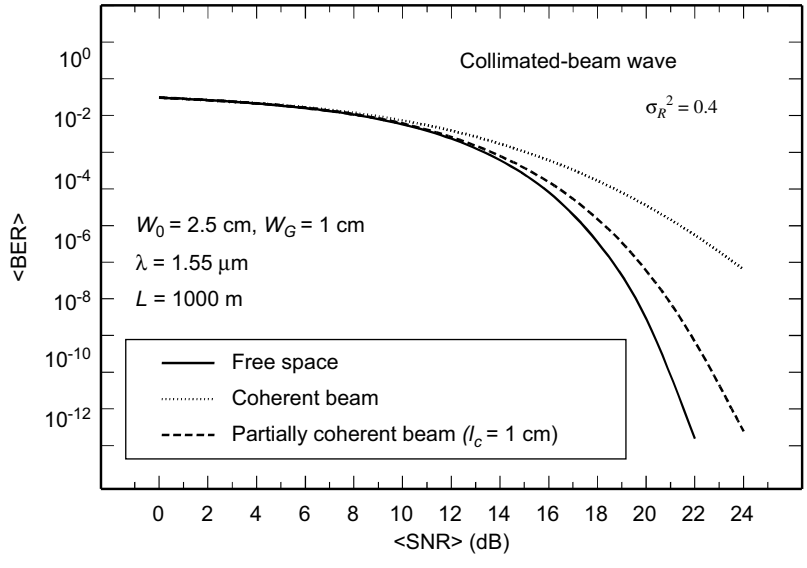

Figure 16.11 Probability of error (BER) for a beam in free space, a coherent beam, and a partially coherent beam as a function of mean SNR. Atmospheric-induced irradiance fluctuations are considered weak.

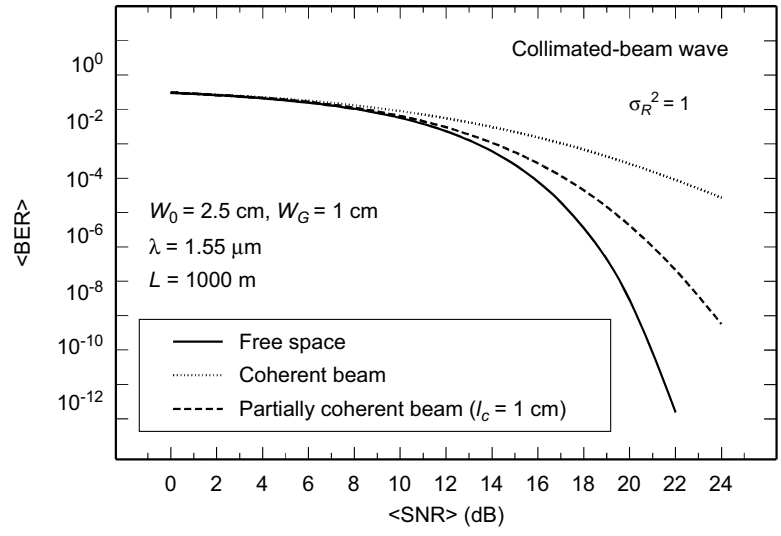

Figure 16.12 Same as Fig. 16.11 for the case of moderate irradiance fluctuations.

16.8 Ladar Model in Free Space

The recent model developed by Korotkova et al. [23,24] for improving the bit error rate (BER) of a FSO system has also been developed for laser radar systems involving the reflection of a coherent beam from an optically rough target [21,22]. In a typical laser radar (lader) application, the ladar beam wave is propagated through atmospheric turbulence to a target that subsequently reflects the optical wave back to the plane of the transmitter/receiver where the return wave is detected (see also Chap. 13). The phase of the target-illumination beam is distorted by atmospheric turbulence along the path, which is further distorted by the target and then distorted again by the same atmospheric turbulence along the return path. In addition to atmospheric conditions, therefore, the target surface plays an important role in determining the nature of the return beam. For example, the surfaces of most targets are considered rough on the scale of an optical wavelength, causing the reflected wave to be scattered in all directions. Hence, the reflected optical wave back at the pupil plane of the receiver consists of many coherent components, each arising from a different microscopic element of the surface. Interference of the coherent components results in a granular pattern of irradiance at the receiver pupil plane that is known as speckle. The correlation area of the speckle in the pupil plane or image plane is important because it may be used to identify certain target characteristics and/or atmospheric parameters.

Surface roughness is usually defined in terms of surface height deviations from some average value. For random surfaces, it has been customary to start with a Gaussian height model [25], although Stover [26] suggests this may not be necessary. To distinguish between surfaces with the same surface height variations, it is useful to also define a characteristic transverse parameter called the *correlation*

radius l_c. The correlation radius is typically associated with a model for the surface auto-correlation function, which for tractability reasons is also taken in most cases to be a Gaussian function (i.e., the Gaussian Schell-model). However, the target surface can equally well be characterized by the Fourier transform of the autocorrelation function known as the power spectral density (PSD). Use of the PSD has certain computational advantages over the autocorrelation function—in particular, more tractable and general models of surface roughness can be generated with the PSD approach.

Below we develop a theoretical model for a rough surface by treating it like a combination of smooth finite plane reflector and thin random phase screen (Chap. 15). The target acts like a deep random phase screen for the case of a fully diffuse (Lambertian) surface and becomes a continually weakening phase screen as the target surface becomes smoother. In Section 16.9 we extend the analysis to include the effects of optical turbulence.

16.8.1 Free-space analysis

A schematic for the laser radar system under study is provided in Fig. 16.13. We illustrate the two-way propagation path in an "unfolded" manner for clarity and characterize the finite target of radius W_R by the combination of a (finite) Gaussian lens (mirror) and thin random phase screen.

We will develop beam characteristics for both the pupil plane of the receiver lens at distance $2L$ from the transmitter (input plane) and in the plane of the detector at distance L_f behind the front receiver lens (see Fig. 16.13). The propagation path up to the pupil plane (*pp*) is characterized by the *ABCD* ray matrix is

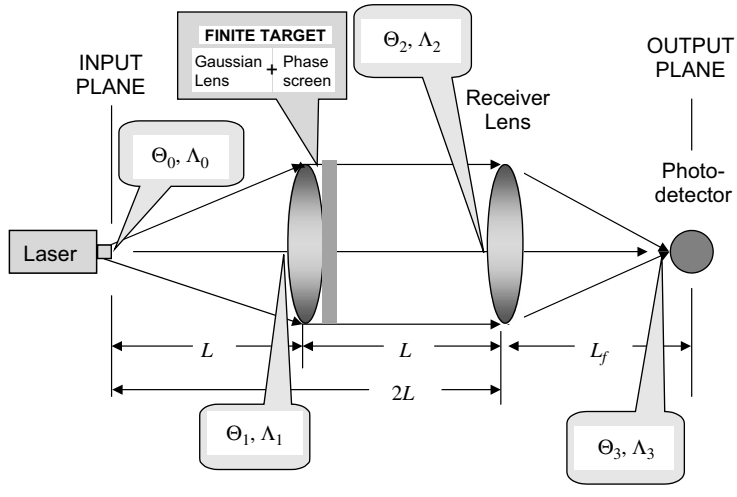

Figure 16.13 Schematic of laser radar configuration (unfolded) for reflection from a rough target.

$$\begin{pmatrix} A_{pp} & B_{pp} \\ C_{pp} & D_{pp} \end{pmatrix} = \begin{pmatrix} 1 & L \\ 0 & 1 \end{pmatrix} \begin{pmatrix} 1 & 0 \\ i\alpha_R & 1 \end{pmatrix} \begin{pmatrix} 1 & L \\ 0 & 1 \end{pmatrix} = \begin{pmatrix} 1 + i\alpha_R L & L + L(1 + i\alpha_R L) \\ i\alpha_R & 1 + i\alpha_R L \end{pmatrix}, \tag{87}$$

where $\alpha_R = 2/kW_R^2$. We also characterize the finite size of the target radius W_R by

$$\Omega_R = \frac{2L}{kW_R^2}. \tag{88}$$

Beam parameters Θ_0, Λ_0 and Θ_1, Λ_1 shown in Fig. 16.13 are defined by Eqs. (1) and (2). Here, however, beam parameters Θ_2, Λ_2 are defined by

$$\begin{aligned} z = 2L^-: \quad \Theta_2 &= \frac{1 + \overline{\Theta}_1}{(1 + \overline{\Theta}_1)^2 + (\Lambda_1 + \Omega_R)^2} = 1 + \frac{L}{F_2}, \\ \Lambda_2 &= \frac{\Lambda_1 + \Omega_R}{(1 + \overline{\Theta}_1)^2 + (\Lambda_1 + \Omega_R)^2} = \frac{2L}{kW_2^2}, \end{aligned} \tag{89}$$

where F_2 and W_2 represent the phase front radius of curvature and beam radius, respectively, of the incident wave on the receiver aperture.

In the detector plane (dp) the overall $ABCD$ matrix becomes (see Section 10.4.1)

$$\begin{pmatrix} A & B \\ C & D \end{pmatrix} = \begin{pmatrix} 1 & L_f \\ 0 & 1 \end{pmatrix} \begin{pmatrix} 1 & 0 \\ i\alpha_G & 1 \end{pmatrix} \begin{pmatrix} A_{pp} & B_{pp} \\ C_{pp} & D_{pp} \end{pmatrix} = \begin{pmatrix} A_{pp} + (C_{pp} + i\alpha_G A_{pp})L_f & B_{pp} + (D_{pp} + i\alpha_G B_{pp})L_{pp} \\ C_{pp} + i\alpha_G A_{pp} & D_{pp} + i\alpha_G B_{pp} \end{pmatrix}. \tag{90}$$

Hence, based on results developed in Section 10.4.1, it is convenient to define another set of beam parameters that characterize the Gaussian beam in the plane of the photodetector, viz.,

$$\begin{aligned} \Theta_3 &= \frac{L}{L_f}\left[\frac{L/L_f - L/F_G + \overline{\Theta}_2}{(L/L_f - L/F_G + \overline{\Theta}_2)^2 + (\Lambda_2 + \Omega_G)^2}\right] = 0, \\ \Lambda_3 &= \frac{L}{L_f}\left[\frac{\Lambda_2 + \Omega_G}{(L/L_f - L/F_G + \overline{\Theta}_2)^2 + (\Lambda_2 + \Omega_G)^2}\right] = \frac{L}{(\Lambda_2 + \Omega_G)L_f}, \end{aligned} \tag{91}$$

where F_G and W_G denote the focal length and aperture radius of the receiver lens and

$$\Omega_G = \frac{2L}{kW_G^2}. \tag{92}$$

16.8.2 Mutual coherence function: pupil plane

In the plane of the receiver the free-space model for the optical field is

$$\begin{aligned} U(\mathbf{r}, 2L) &= U_0(\mathbf{r}, 2L)\exp[\Psi_s(\mathbf{r})] \\ &= \frac{1}{A_{pp} + i\alpha_0 B_{pp}}\left(\frac{2\sqrt{\pi}R_s}{k}\right)\exp(2ikL) \\ &\quad \times \exp\left[-\frac{1}{2}\left(\frac{\alpha_0 D_{pp} - iC_{pp}}{A_{pp} + i\alpha_0 B_{pp}}\right)kr^2\right]\exp[\Psi_s(\mathbf{r})], \end{aligned} \tag{93}$$

where R_s is a surface constant defined below and $\Psi_s(\mathbf{r})$ is the random complex phase perturbation induced by the phase screen. The free-space mutual coherence function (MCF) is defined by the ensemble average

$$\begin{aligned} \Gamma_{\text{pp, diff}}(\mathbf{r}_1, \mathbf{r}_2, 2L) &= \langle U_0(\mathbf{r}_1, 2L)U_0^*(\mathbf{r}_2, 2L)\rangle\langle\exp\left[\Psi_s(\mathbf{r}_1) + \Psi_s^*(\mathbf{r}_2)\right]\rangle \\ &= \Gamma_0(\mathbf{r}_1, \mathbf{r}_2, 2L)\exp\left\{-4\pi^2 k^2 \Delta z \int_0^\infty \kappa\Phi_S(\kappa)\right. \\ &\quad \left.\times\left[1 - e^{-\Lambda_2 L\kappa^2/k}J_0(\kappa|\Theta_2\mathbf{p} - 2i\Lambda_2\mathbf{r}|)\right]d\kappa\right\}, \end{aligned} \tag{94}$$

where $\Gamma_0(\mathbf{r}_1, \mathbf{r}_2, 2L) = U_0(\mathbf{r}_1, 2L)U_0^*(\mathbf{r}_2, 2L)$ is the free-space MCF for a smooth finite target. Because it has the same form as Eq. (20), it follows that the evaluation of (94) leads to [see also Eq. (28)]

$$\begin{aligned} \Gamma_{\text{pp, diff}}(\mathbf{r}_1, \mathbf{r}_2, 2L) &= \frac{4\pi R_s^2 W_0^2}{k^2 W_2^2(1 + 4\Lambda_2 q_c)}\exp\left[\frac{ik}{L}\left(\frac{1 - \Theta_2 + 4\Lambda_2 q_c}{1 + 4\Lambda_2 q_c}\right)\mathbf{r}\cdot\mathbf{p}\right] \\ &\quad \times \exp\left[-\frac{2r^2 + \rho^2/2}{W_2^2(1 + 4\Lambda_2 q_c)}\right]\exp\left[-\left(\frac{\Theta_2^2 + \Lambda_2^2}{1 + 4\Lambda_2 q_c}\right)\left(\frac{\rho^2}{l_c^2}\right)\right], \end{aligned} \tag{95}$$

where we have introduced the nondimensional surface "roughness" parameter $q_c = L/kl_c^2$. The *surface reflection parameter* appearing in (95) leads to the limiting cases

$$R_s^2 = \begin{cases} k^2/4\pi & \text{(smooth target)} \\ T_0^2/\pi l_c^2 & \text{(diffuse target),} \end{cases} \tag{96}$$

where T_0^2 is the reflection coefficient of the target and the fully diffuse target case arises in the limit $l_c \to 0$. In the limit $l_c \to \infty$, Eq. (95) reduces to that for a smooth target [recall Eq. (40) in Chap. 13]

$$\Gamma_0(\mathbf{r}_1, \mathbf{r}_2, 2L) = \frac{W_0^2}{W_2^2(1 + \Omega_R/\Lambda_1)} \exp\left(-\Lambda_2 \frac{kr^2}{L}\right) \exp\left(-\Lambda_2 \frac{k\rho^2}{4L}\right) \exp\left(\frac{ik}{L} \overline{\Theta}_2 \mathbf{r} \cdot \mathbf{p}\right), \tag{97}$$

where $\overline{\Theta}_2 = 1 - \Theta_2$.

The first exponential function in the second line of (95) describes the profile of the mean irradiance for the reflected partially coherent beam wave. In particular, if W_2 is the beam radius in the case of a smooth finite target, then the increased beam size caused by the rough surface is related by

$$W_{2,\,\mathrm{diff}} = W_2 \sqrt{1 + 4\Lambda_2 q_c}. \tag{98}$$

The coherence properties of the echo wave can be deduced from the magnitude of the complex degree of coherence defined by

$$\mathrm{DOC}_{\,\mathrm{pp,\,diff}}(\rho, 2L) = \frac{|\Gamma_{\,\mathrm{pp,\,diff}}(\mathbf{r}_1, \mathbf{r}_2, 2L)|}{\sqrt{\Gamma_{\,\mathrm{pp,\,diff}}(\mathbf{r}_1, \mathbf{r}_1, 2L)\Gamma_{\,\mathrm{pp,\,diff}}(\mathbf{r}_2, \mathbf{r}_2, 2L)}}, \tag{99}$$

which reduces to

$$\mathrm{DOC}_{\,\mathrm{pp,\,diff}}(\rho, 2L) = \exp\left[-\left(\frac{\Theta_2^2 + \Lambda_2^2}{1 + 4\Lambda_2 q_c}\right) \frac{\rho^2}{l_c^2}\right] = \exp\left(-\frac{\rho^2}{\rho_{\mathrm{pp,\,speckle}}^2}\right). \tag{100}$$

From this last expression, we can define the speckle radius in the pupil plane by

$$\rho_{\mathrm{pp,\,speckle}} = \sqrt{\frac{(1 + 4\Lambda_2 q_c) l_c^2}{\Theta_2^2 + \Lambda_2^2}}. \tag{101}$$

In the limit of a fully diffuse target we find that (101) reduces further to

$$\rho_{\mathrm{pp,\,speckle}} = \lim_{l_c \to 0} \sqrt{\frac{(1 + 4\Lambda_2 q_c) l_c^2}{\Theta_2^2 + \Lambda_2^2}} = \frac{\sqrt{2}\lambda L}{\pi W_R} \sqrt{1 + \frac{W_R^2}{W_1^2}}. \tag{102}$$

Equations (101) and (102) are more general than the classic result of Goodman [27] because (101) involves the spatial roughness of the target and (102) includes the size of the illumination beam W_1 in relation to the target radius W_R. However, in the case of an unresolved target ($W_R \ll W_1$), Eq. (102) reduces to Goodman's result[1]

$$\rho_{\mathrm{pp,\,speckle}} = \frac{\sqrt{2}\lambda L}{\pi W_R} \qquad \text{(unresolved target)}. \tag{103}$$

A related quantity used in accessing lidar performance is the number of speckle cells N_S captured by the receiver telescope [28,29]. Based on (103), the number of speckle cells on the receiver lens for an unresolved diffuse target is

[1]Equation (103) has a slightly different multiplicative constant than Goodman's classic result.

$$N_s = 1 + \frac{S_{\text{lens}}}{S_{\text{speckle}}} = \frac{1 + 2\Omega_G\Omega_R}{2\Omega_G\Omega_R} \qquad \text{(unresolved target)}, \tag{104}$$

where S_{lens} and S_{speckle} denote the receiver aperture area and speckle correlation area, respectively. In the limiting case of a small target and/or small receiver lens, we have $\Omega_G\Omega_R \to \infty$ and the number of speckle cells reduces to one.

16.8.3 Speckle size: image plane

In the plane of the detector at distance L_f behind the front receiver lens (see Fig. 16.13) we will only calculate the speckle size of the echo wave by use of the modulus of the complex degree of coherence.

The modulus of the complex degree of coherence is related to the wave structure function (WSF) by $D_s(\mathbf{r}_1, \mathbf{r}_2, 2L + L_f)$ by

$$\text{DOC}_{\text{ip, diff}}(\boldsymbol{\rho}, 2L + L_f) = \exp\left[-\frac{1}{2} D_s(\mathbf{r}_1, \mathbf{r}_2, 2L + L_f)\right], \tag{105}$$

where the WSF is defined by [22,23,30]

$$\begin{aligned} D_s(\mathbf{r}_1, \mathbf{r}_2, 2L + L_f) = 4\pi^2 k^2 \Delta z \text{Re} \int_0^\infty \kappa \Phi_s(\kappa) \exp\left[-\left(\frac{\Theta_2^2 + \Lambda_2^2\Omega_G}{\Lambda_2 + \Omega_G}\right)\frac{L\kappa^2}{k}\right] \\ \times \left\{ I_0\left[\frac{2L\Theta_2 r_1 \kappa}{(\Lambda_2 + \Omega_G)L_f}\right] + I_0\left[\frac{2L\Theta_2 r_2 \kappa}{(\Lambda_2 + \Omega_G)L_f}\right] \right. \\ \left. - J_0\left[\kappa\left|\frac{L\Lambda_2 \mathbf{p}}{(\Lambda_2 + \Omega_G)L_f} + \frac{2iL\Theta_2 \mathbf{r}}{(\Lambda_2 + \Omega_G)L_f}\right|\right]\right\} d\kappa. \end{aligned} \tag{106}$$

Hence, upon evaluation of the integral in (106), Eq. (105) simplifies to

$$\text{DOC}_{\text{ip, diff}}(\boldsymbol{\rho}, 2L + L_f) = \exp\left\{ -\left[\frac{1}{1 + 4q_c\left(\frac{\Theta_2^2 + \Lambda_2\Omega_G}{\Lambda_2 + \Omega_G}\right)}\right]\left[\frac{(\Theta_2^2 + \Lambda_2^2)L^2}{(\Lambda_2 + \Omega_G)^2 L_f^2}\right]\left(\frac{\rho^2}{l_c^2}\right)\right\}, \tag{107}$$

from which we deduce the speckle size in the image plane (i.e., detector plane)

$$\rho_{\text{ip, speckle}} = \frac{l_c L_f (\Lambda_2 + \Omega_G)}{L\sqrt{\Theta_2^2 + \Lambda_2^2}} \sqrt{1 + 4q_c\left(\frac{\Theta_2^2 + \Lambda_2\Omega_G}{\Lambda_2 + \Omega_G}\right)}. \tag{108}$$

In the limiting case of a finite, fully diffuse, unresolved target, we obtain the speckle size expression

$$\rho_{\text{ip, speckle}} = 1.27\left(\frac{\lambda L_f}{D_G}\right)\sqrt{1+\Omega_G\Omega_R} \quad \text{(unresolved target)}. \tag{109}$$

16.9 Ladar Model in Optical Turbulence

We now consider the ladar model in the presence of optical turbulence, which we assume is statistically independent of the fluctuations associated with the random rough target [30]. Below we will examine the effect of optical turbulence on the speckle size in the pupil plane of the receiver and also its effect on the scintillation index in this plane.

16.9.1 Speckle size: pupil plane

The modulus of the complex degree of coherence (100) in the presence of optical turbulence now takes the form

$$\text{DOC}_{\text{pp, diff}}(\rho, 2L) = \exp\left[-\left(\frac{\Theta_2^2+\Lambda_2^2}{1+4\Lambda_2 q_c}\right)\frac{\rho^2}{l_c^2} - \frac{1}{2}D_{\text{atm}}(\rho, 2L)\right], \tag{110}$$

where $D_{\text{atm}}(\rho, 2L)$ is the WSF of the reflected optical wave (due to atmospheric effects) in the plane of the receiver. By writing the WSF in the form

$$D_{\text{atm}}(\rho, 2L) = 2\left(\frac{\rho}{\rho_0}\right)^{5/3} \cong 2\left(\frac{\rho}{\rho_0}\right)^2, \tag{111}$$

where ρ_0 is the spatial coherence radius, we find that, by substituting this last expression into (110), we can identify an approximation of the implied average speckle size of the partially coherent beam by the expression

$$\rho_{\text{pp, speckle}} = \left[\left(\frac{\Theta_2^2+\Lambda_2^2}{1+4\Lambda_2 q_c}\right)\frac{1}{l_c^2} + \frac{1}{\rho_0^2}\right]^{-1/2} \quad \text{(unresolved target)}. \tag{112}$$

In the limiting case of a fully diffuse target, it follows that Eq. (112) reduces to

$$\rho_{\text{pp, speckle}} = \frac{\sqrt{2}\lambda L/\pi W_R}{\sqrt{1+2(\lambda L/\pi W_R\rho_0)^2}} \quad \text{(unresolved target)}, \tag{113}$$

from which we deduce the average number of speckle cells

$$N_s = 1 + \frac{S_{\text{lens}}}{S_{\text{speckle}}} = \frac{1+2\Omega_G\Omega_R + 2(\lambda L/\pi W_R\rho_0)^2}{2\Omega_G\Omega_R} \quad \text{(unresolved target)}. \tag{114}$$

By comparison with Eqs. (103) and (104), we see that the presence of atmospheric turbulence tends to reduce the speckle size (113) and hence, increase the number of speckle cells (114), provided the spatial coherence radius satisfies $\rho_0 < \lambda L/\pi W_R$.

In the case of a resolved fully diffuse target, it can be shown that the average speckle size is approximated by

$$\rho_{\text{pp, speckle}} = \frac{\sqrt{2}\lambda L}{\pi W_R}\sqrt{\frac{1 + W_R^2/W_1^2}{1 + 2(1 + W_R^2/W_1^2)(\lambda L/\pi W_R \rho_0)^2}} \quad \text{(resolved target)}, \tag{115}$$

and the corresponding number of speckle cells is

$$N_s = \frac{1 + 2\Omega_G\Omega_R + 2(1 + W_R^2/W_1^2)(\lambda L/\pi W_R\rho_0)^2}{2\Omega_G\Omega_R(1 + W_R^2/W_1^2)} \quad \text{(resolved target)}. \tag{116}$$

Both (115) and (116) are dependent on the WSF approximation given by (111).

Equation (116) is similar to an expression developed by Drobinski et al. [29] for a resolved target, although Drobinski et al. used an expression for the long-term spot size of the illumination beam to characterize the effective size of the target. In that analysis it was also assumed that the spatial coherence radius ρ_0 is twice that of a spherical wave propagating over a one-way path of length L. The average number of speckle cells in the pupil plane of a ladar receiver system was suggested by Drobinski et al. to be a useful optical method for measuring path-averaged values of the refractive-index structure parameter C_n^2. The proposed method depends on using the gamma distribution with parameter m, equal to the reciprocal of the integrated irradiance over the receiver aperture, and equating the parameter m of this model with the number of speckle cells. Such a method for measuring the path-averaged value of C_n^2 with a 10.6-μm coherent ladar in a direct detection mode has in fact been validated [29].

16.9.2 Scintillation index: slow detector case

In developing expressions for the scintillation index in the pupil plane of the receiver, we consider only the case of an incident *spherical wave*. However, we will take into account the response time of the detector τ_D and the coherence time of the target surface τ_S caused by temporal variations of the surface (see also Sections 16.5 and 16.6). To begin, we consider the *slow detector case* in which $\tau_D \gg \tau_S$.

Following the approach used in Section 16.5.1, we define effective beam parameters associated with the echo beam from the rough surface by

$$\Theta_{2e} = \frac{\Theta_2}{1 + 4\Lambda_2 q_c}, \qquad \Lambda_{2e} = \frac{\Lambda_2[1 + 4q_c/(\Lambda_1 + \Omega_R)]}{1 + 4\Lambda_2 q_c}. \tag{117}$$

Equations (117) are for the general case of an incident Gaussian-beam wave on the target. For the special case of an incident spherical wave considered here, we find that $\Theta_1 = \Lambda_1 = 0$. Also, for this case we have $\Theta_2 = 2/(4 + \Omega_R^2)$ and $\Lambda_2 = \Omega_R/(4 + \Omega_R^2)$. Like the single-pass propagation case, the effective beam parameters (117) are deduced by comparing the MCF for a smooth target (97) with the MCF for a rough target (95). Under weak irradiance fluctuations in a

bistatic ladar system, the resulting (on-axis) scintillation index of a reflected spherical wave from a smooth target is [recall Eq. (98) in Chap. 13]

$$\sigma_I^2(0, 2L) = 2\sigma_{I,\,\text{beam}}^2(0, L), \tag{118}$$

where $\sigma_{I,\,\text{beam}}^2(0, L)$ is defined by Eq. (101) in Chap. 13. Under the assumption of a Kolmogorov spectrum, the corresponding scintillation index of a reflected spherical wave from a rough target in the presence of optical turbulence is

$$\sigma_{I,\,\text{atm}}^2(0, 2L) = 7.72\sigma_R^2 \text{Re}\left[i^{5/6}{}_2F_1\left(-\frac{5}{6}, \frac{11}{6}; \frac{17}{6}; 1 - \Theta_{2e} + i\Lambda_{2e}\right) - \frac{11}{16}\Lambda_{2e}^{5/6}\right], \tag{119}$$

where we have formally replaced the beam parameters Θ_2 and Λ_2 with the effective beam parameters (117).

We plot Eq. (119) in Fig. 16.14 as a function of target size parameter Ω_R and several cases of a partially rough surface ranging from a smooth reflector (solid curve) to a fully diffuse target (dotted curve). Note that for small targets ($\Omega_R \gg 1$), all curves merge to the same scintillation index, but for large targets ($\Omega_R \ll 1$), each curve saturates to a different level depending on the surface roughness correlation length. That is, the rough surface produces an aperture-averaging effect on the return wave with the greatest reduction in scintillation always coming from the largest target.

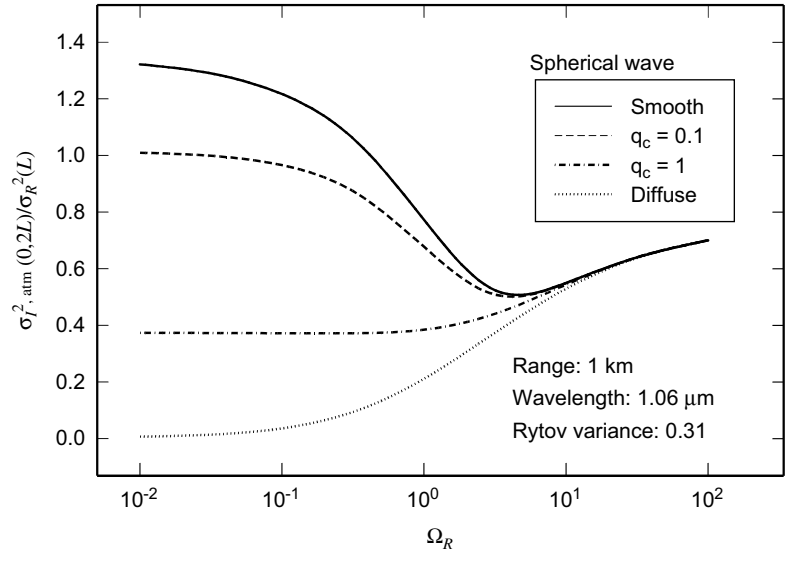

Figure 16.14 Scaled scintillation index of a reflected spherical wave from a partially diffuse target as a function of normalized target size.

16.9.3 Scintillation index: fast detector case

The scattering properties of physical diffuse targets such as atmospheric aerosols, a sea surface, or a rough surface can vary with time when scanned by a laser radar. If the coherence time of the detector is much shorter than the coherence time of the rough target surface (i.e., if $\tau_D \ll \tau_S$), the detector will be sensitive to irradiance fluctuations of the target. In this case the phase screen model leads to the (on-axis) scintillation index (ignoring atmospheric effects) defined by

$$\begin{aligned}\sigma^2_{I,\,\mathrm{diff}}(0,2L) &= 8\pi^2 k^2 \Delta z \int_0^\infty \kappa \Phi_S(\kappa) e^{-\Lambda_2 L\kappa^2/k}\left[1-\cos\left(\frac{\Theta_2 L\kappa^2}{k}\right)\right]d\kappa \\ &= 1-\frac{1+4\Lambda_2 q_c}{(1+4\Lambda_2 q_c)^2+16\Theta_2^2 q_c^2},\end{aligned} \tag{120}$$

where we have used the Gaussian spectrum model (18). Note that this expression has the same form as that given by Eq. (71) for one-way propagation through a diffuser.

The integrated irradiance at the detector is described by

$$E(\mathbf{r},2L) = \frac{1}{T}\int_{-T/2}^{T/2} I(\mathbf{r},2L;t)dt, \tag{121}$$

where $I(\mathbf{r},2L;t)$ is the instantaneous irradiance and T is the integration time. By following the analysis provided in Section 16.6.2 for the one-way propagation path, we are once again led to the variance of the integrated irradiance

$$\sigma^2_{I,E}(0,2L) = \sigma^2_{I,\,\mathrm{diff}}(0,2L)\left[\frac{\tau_S}{\tau_D}+\frac{1}{2}\left(\frac{\tau_S}{\tau_D}\right)^2\left(e^{-2\tau_D/\tau_S}-1\right)\right]. \tag{122}$$

Consequently, the scintillation index arising from the combined effects of the atmosphere, rough surface, and temporal fluctuations of the surface is

$$\sigma_I^2(0,2L) = \sigma^2_{I,\mathrm{atm}}(0,2L) + \sigma^2_{I,E}(0,2L)\left[1+\sigma^2_{I,\,\mathrm{atm}}(0,2L)\right]. \tag{123}$$

In Figs. 16.15–16.17 we plot the scintillation index (123) as a function of normalized target size Ω_R and several cases of surface roughness correlation parameter. In each figure we take a different ratio of τ_S/τ_D. The case $\tau_S/\tau_D = 0.1$ illustrated in Fig. 16.15 corresponds to a slow detector whereas the case $\tau_S/\tau_D = 10$ shown in Fig. 16.17 corresponds to a fast detector. Here we see that the combination of target size and temporal coherence ratios has a significant effect on the implied scintillation index, particularly for large targets ($\Omega_R \ll 1$). In all cases, of course, the smooth target leads to the same scintillation index.

16.10 Summary and Discussion

We have developed analytic expressions for several statistical quantities involving the propagation of a (spatially) partially coherent beam through optical turbulence.

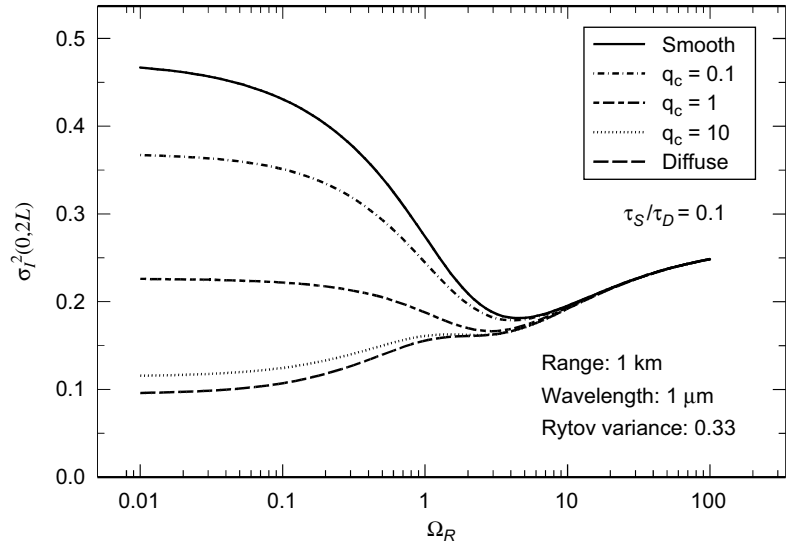

Figure 16.15 Scintillation index of a reflected spherical wave from a partially diffuse surface with $\tau_S/\tau_D = 0.1$.

Our primary model for the partially coherent beam is based on a diffuser at the exit aperture of the transmitter that we treat like a thin random phase screen (see Chap. 15). Doing so permits us to describe the phase screen characteristics by a power spectrum model rather than by the autocorrelation function depicting the diffuser correlation width. In particular, the scintillation model developed here using a Gaussian spectrum for the phase screen is significantly simpler than those arising from a more conventional approach using a Gaussian Schell-model.

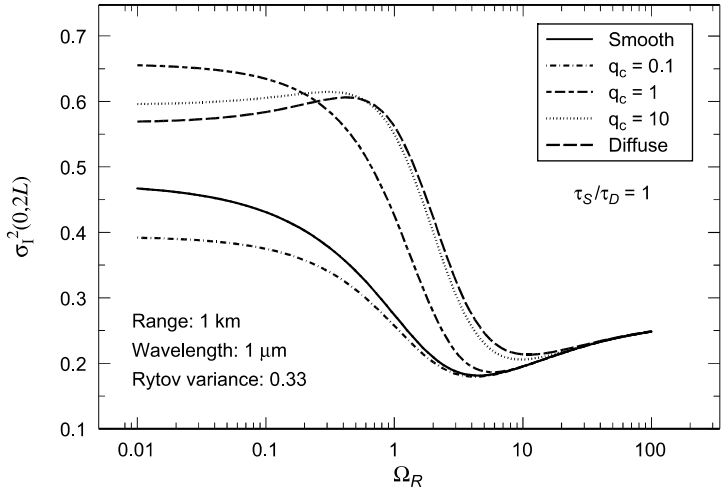

Figure 16.16 Same as Fig. 16.15 with $\tau_S/\tau_D = 1$.

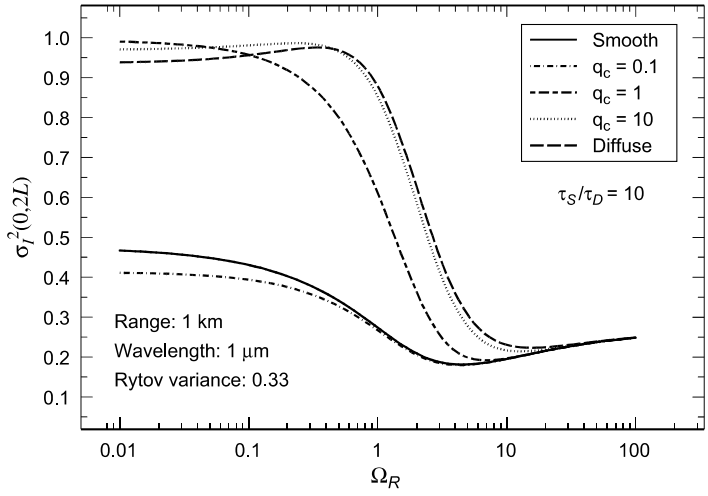

Figure 16.17 Same as Fig. 16.15 with $\tau_S/\tau_D = 10$.

Moreover, the spectrum model for the phase screen can be readily replaced with other spectrum models like a power-law model.

Although the analysis concerning a partially coherent beam is still an open area of research, it has been demonstrated that the use of such a beam in certain free-space optical communication links can be effective in reducing the fade probability, and hence, the bit error rate. Preliminary findings seem to favor propagation channels operating under weak-to-moderate irradiance fluctuations rather than under strong fluctuations.

The same partially coherent beam model has also been adapted to certain laser radar applications involving reflections from a rough surface. The advantage in the model is that, by changing the surface roughness correlation radius, the target can take on characteristics ranging from those of a smooth reflector to those of a fully diffuse target (see Chap. 13). Combined with the use of *ABCD* ray matrices, we have developed estimates for the speckle size and number of speckle cells in both the pupil plane of the receiver and in the image plane (detector plane). Moreover, we have obtained expressions for the scintillation index in both the "slow detector" case and the "fast detector" case. In all instances, we assume that surface height fluctuations of the target are sufficiently large that the phase variance of the reflected wave is also large (much more than 2π radians). In such cases the phase lateral correlation width is directly related to the lateral correlation radius of the surface heights. Last, we have ignored any change in polarization that may arise from target reflections.

16.11 Worked Examples

Example 1: A collimated beam of diameter 5 cm operating at $\lambda = 1.55\ \mu$m is passed through a diffuser at the transmitter characterized by $l_c = 2$ cm.

If the beam propagates through free space to a receiver located 1 km from the transmitter, calculate

(*a*) the average number of speckle cells at the exit aperture of the diffuser.
(*b*) the average speckle radius in the pupil plane.
(*c*) the average speckle radius in the pupil plane for a strong diffuser.

Solution: We first compute the quantities

$$q_c = \frac{L}{kl_c^2} = 0.62,$$

$$W_1 = W_0\sqrt{\Theta_0^2 + \Lambda_0^2} = 3.19\,\text{cm}, \qquad W_{\text{pp, diff}} = W_1\sqrt{1 + 4\Lambda_1 q_c} = 4.72\,\text{cm}.$$

(*a*) $N_S = 1 + \dfrac{2W_0^2}{l_c^2} = 4.13$

(*b*) $\rho_{\text{pp, speckle}} = \dfrac{l_c}{W_0} W_{\text{pp, diff}} = 3.8\,\text{cm}.$

(*c*) $\rho_{\text{pp, speckle}} = \dfrac{2\sqrt{2}L}{kW_0} = 2.8\,\text{cm}.$

❑

Example 2: If the beam in Example 1 above is collected by a receiver aperture of diameter 8 cm and $L_f = 16\,\text{cm}$, what is the spot radius of the beam and speckle radius in the image plane of the receiver system?

Solution: To begin, we calculate

$$\Lambda_2 = \frac{L}{L_f(\Lambda_1 + \Omega_G)} = 15{,}729.$$

Consequently, the spot radius of the beam in the image plane is

$$W_2 = \sqrt{\frac{2L}{k\Lambda_2}} = 1.6\,\mu\text{m}.$$

The radius of the image plane speckle is then calculated from

$$\rho_{\text{ip, speckle}} = \left(\frac{l_c}{W_0}\right)\left(\frac{W_1}{W_G}\right)W_2\sqrt{1 + 4q_c\left(\frac{\Theta_1^2 + \Lambda_1\Omega_G}{\Lambda_1 + \Omega_G}\right)} \cong 1.6\,\mu\text{m}.$$

❑

Problems

Section 16.3

1. Show that evaluation of the double integral in Eq. (9) leads to

$$\Gamma_{\text{pp, diff}}(\mathbf{r}_1, \mathbf{r}_2, L) = \frac{W_0^2}{W_1^2(1 + 4\Lambda_1 q_c)} \exp\left[\frac{ik}{L}\left(\frac{1 - \Theta_1 + 4\Lambda_1 q_c}{1 + 4\Lambda_1 q_c}\right)\mathbf{r} \cdot \mathbf{p}\right] \times \exp\left[-\frac{2r^2 + \rho^2/2}{W_1^2(1 + 4\Lambda_1 q_c)}\right] \exp\left[-\left(\frac{\Theta_1^2 + \Lambda_1^2}{1 + 4\Lambda_1 q_c}\right)\left(\frac{\rho^2}{l_c^2}\right)\right],$$

   where $\mathbf{p} = \mathbf{r}_1 - \mathbf{r}_2, \rho = |\mathbf{p}|, \mathbf{r} = (1/2)(\mathbf{r}_1 + \mathbf{r}_2)$, and $q_c = L/kl_c^2$.

2. From the expression given in Prob. 1, deduce the DOC

$$\begin{aligned}\text{DOC}_{\text{pp, diff}}(\rho, L) &= \frac{|\Gamma_{\text{pp, diff}}(\mathbf{r}_1, \mathbf{r}_2, L)|}{\sqrt{\Gamma_{\text{pp, diff}}(\mathbf{r}_1, \mathbf{r}_1, L)\Gamma_{\text{pp, diff}}(\mathbf{r}_2, \mathbf{r}_2, L)}} \\ &= \exp\left[-\left(\frac{\Theta_1^2 + \Lambda_1^2}{1 + 4\Lambda_1 q_c}\right)\frac{\rho^2}{l_c^2}\right].\end{aligned}$$

3. Prove Eq. (16), i.e., show that the number of speckle cells at the source remains a constant.

4. Show that, in the limit of a strong diffuser, the average speckle radius reduces to

$$\rho_{\text{pp, speckle}} = \lim_{l_c \to 0} \sqrt{\frac{l_c^2(1 + 4\Lambda_1 q_c)}{\Theta_1^2 + \Lambda_1^2}} = \frac{\sqrt{2}\lambda L}{\pi W_0}.$$

Section 16.4

5. Given the Gaussian spectrum model

$$\Phi_S(\kappa) = \frac{\langle n_1^2 \rangle l_c^3}{8\pi\sqrt{\pi}} \exp\left(-\frac{l_c^2 \kappa^2}{4}\right),$$

   and the normalization factor

$$\frac{\sqrt{\pi}\langle n_1^2 \rangle k^2 l_c \Delta z}{1 + 4\Lambda_1 q_c} = 1,$$

show by direct evaluation that

$$(a)\ \sigma^2_{r,\,\mathrm{diff}}(\mathbf{r}, L) = 2\pi^2 k^2 \Delta z \int_0^\infty \kappa \Phi_S(\kappa) e^{-\Lambda_1 L\kappa^2/k}[I_0(2\Lambda_1 r\kappa) - 1]d\kappa$$

$$= \exp\left[\frac{4\Lambda_1^2 r^2}{(1 + 4\Lambda_1 q_c) l_c^2}\right] - 1.$$

$$(b)\ T_{\mathrm{diff}}(L) = 4\pi^2 k^2 \Delta z \int_0^\infty \kappa \Phi_S(\kappa)\left(1 - e^{-\Lambda_1 L\kappa^2/k}\right)d\kappa = 4\Lambda_1 q_c,$$

$$(c)\ \Delta^2_{\mathrm{diff}}(\mathbf{r}_1, \mathbf{r}_2, L) = 4\pi^2 k^2 \Delta z \int_0^\infty \kappa \Phi_S(\kappa) e^{-\Lambda_1 L\kappa^2/k}$$

$$\times [I_0(2\Lambda_1 r_1\kappa) + I_0(2\Lambda_1 r_2\kappa) - 2J_0(\kappa|\Theta_1\mathbf{p} - 2i\Lambda_1\mathbf{r}|)]d\kappa$$

$$= 2\left(\frac{\Theta_1 + \Lambda_1^2}{1 + 4\Lambda_1 q_c}\right)\frac{\rho^2}{l_c^2} - \frac{4i\Theta_1 \mathbf{p}\cdot\mathbf{r}}{(1 + 4\Lambda_1 q_c) l_c^2}.$$

6. From Eq. (22) and the results of Prob. 5, deduce the MCF given in Prob. 1.

7. Given the *ABCD* matrix (29) for the Gaussian beam in the image plane

$$\begin{pmatrix} A & B \\ C & D \end{pmatrix} = \begin{pmatrix} 1 + i\alpha_G L_f & L + L_f(1 + i\alpha_G L) \\ i\alpha_G & 1 + i\alpha_G L \end{pmatrix},$$

where $\alpha_G = 2/kW_G^2 + i/F_G$, use the relation

$$\frac{\alpha_0 D - iC}{A + i\alpha_0 B} = \frac{2}{kW_2^2} + i\frac{1}{F_2}$$

to deduce an expression for the free-space spot size W_2 of the beam in this plane.

8. Given the ratio of speckle radii between the image plane and the pupil plane

$$\frac{\rho_{\mathrm{ip,\,speckle}}}{\rho_{\mathrm{pp,\,speckle}}} = \left(\frac{W_1}{W_G}\right)\left(\frac{W_{\mathrm{ip,\,diff}}}{W_{\mathrm{pp,\,diff}}}\right),$$

show that in the limit of a strong diffuser, it reduces to Eq. (43).

9. Given the beam characteristics presented in Example 1 in Section 16.11, what is the long-term beam radius under atmospheric turbulence conditions in which the structure constant is $C_n^2 = 2 \times 10^{-14}\ \mathrm{m}^{-2/3}$?
Ans. 4.72 cm

Section 16.5

10. Given the effective beam parameters defined by

$$\Theta_{ed} = \frac{\Theta_1}{1 + 4\Lambda_1 q_c}, \qquad \Lambda_{ed} = \frac{\Lambda_1 N_S}{1 + 4\Lambda_1 q_c},$$

show that they can also be defined in terms of the transmitter beam parameters and number of speckle cells N_S as

$$\Theta_{ed} = \frac{\Theta_0}{\Theta_0^2 + \Lambda_0^2 N_S}, \qquad \Lambda_{ed} = \frac{\Lambda_0 N_S}{\Theta_0^2 + \Lambda_0^2 N_S}.$$

11. Given a collimated beam of diameter 3 cm at the transmitter and $\lambda = 10.6\,\mu\text{m}$, calculate the on-axis scintillation index at distance 3 km from the transmitter if it is first passed through a diffuser with $l_c = 1$ cm. Assume $C_n^2 = 3 \times 10^{-13}\,\text{m}^{-2/3}$ and neglect the effects of inner and outer scale. For a strong diffuser ($l_c \to 0$), what is the resulting scintillation index?

12. Given the conditions cited in Prob. 11, what is the total off-axis scintillation index at radial position $r/W_1 = 0.8$ for $l_c = 1$ cm? for a strong diffuser?

Section 16.6

13. Use the Gaussian spectrum (18) and Eq. (72) to show that

$$\sigma_{I,\text{diff}}^2(0, L) = 8\pi^2 k^2 \Delta z \int_0^\infty \kappa \Phi_S(\kappa) e^{-\Lambda_1 L \kappa^2/k} \left[1 - \cos\left(\frac{\Theta_1 L \kappa^2}{k}\right)\right] d\kappa$$

$$= 1 - \frac{1 + 4\Lambda_1 q_c}{(1 + 4\Lambda_1 q_c)^2 + 16\Theta_1^2 q_c^2}.$$

14. Given the beam and atmospheric characteristics cited in Prob. 11, calculate the longitudinal component of the scintillation index for a detector in which the coherence time of the source and the response time of the detector satisfy
(*a*) $\tau_S/\tau_D = 1$.
(*b*) What is the scintillation index if $\tau_S/\tau_D = 10$?
(*c*) What is the scintillation index if $\tau_S/\tau_D = 0.1$?

Section 16.7

15. Assume the beam and atmospheric conditions used in creating the curves shown in Fig. 16.9. Create similar curves for the cases $q_c = 0.5$ and $q_c = 10$.

16. Consider the beam and atmospheric conditions given in Fig. 16.12. If the correlation length of the diffuser is $l_c = 0.5$ cm, what value of $\langle \text{SNR} \rangle$ is required to produce a probability of error equal to 10^{-9}?

Section 16.8

17. Given a collimated beam of diameter 3 cm at the transmitter and $\lambda = 1.06\,\mu\text{m}$ calculate the free-space spot radius W_2 in the receiver plane of a monostatic system for the reflected beam from a smooth target of diameter 4 cm at distance of 1 km from the transmitter. If the target has a rough surface characterized by $l_c = 1$ cm, what is the free-space spot radius $W_{2,\text{diff}}$?

18. Given the rough target and beam conditions of Prob. 17, calculate the speckle radius of the echo wave in the
    (*a*) Pupil plane of the receiver.
    (*b*) Image plane of the receiver if the receiver lens diameter is 3 cm.
    (*c*) Solve part (*a*) for the case of a fully diffuse target.

Section 16.9

19. Consider a collimated beam of diameter 3 cm at the transmitter and $\lambda = 1.06\,\mu\text{m}$. If the target of diameter 7 cm and $l_c = 1\,\text{cm}$ is located 800 m from the transmitter, estimate the spatial coherence radius of the echo beam back in the plane of the transmitter by use of $\rho_0 = 2/(0.55C_n^2k^2L)^{3/5}$ with $C_n^2 = 2.6 \times 10^{-14}\,\text{m}^{-2/3}$. Then calculate the average number of speckle cells on a receiver lens of diameter 4 cm.

20. Calculate the on-axis scintillation index in a bistatic ladar system for the beam and target in Prob. 19
    (*a*) For a slow detector receiver system.
    (*b*) For a fast detector system with $\tau_S/\tau_D = 10$.

References

1. A. I. Kon and V. I. Tatarskii, "On the theory of the propagation of partially coherent light beams in a turbulent atmosphere," *Radiophys. Quantum Electron.* **15**, 1187–1192 (1972).
2. J. W. Goodman, "Statistical properties of laser speckle patterns," in Laser Speckle and Related Phenomena, J. C. Dainty, ed. (Springer-Verlag, Berlin, 1975).
3. J. Ohtsubo and T. Asakura, "Statistical properties of laser speckle produced in the diffraction field," *Appl. Opt.* **16**, 1742–1753 (1977).
4. M. S. Belenkii and V. L. Mironov, "Turbulent distortions of the spatial coherence of a laser beam," *Sov. J. Quantum Electron.* **7**, 287–290 (1977).
5. J. C. Leader, "Atmospheric propagation of partially coherent radiation," *J. Opt. Soc. Am.* **68**, 175–185 (1978).
6. J. Carl Leader, "Intensity fluctuations resulting from a spatially partially coherent light propagating through atmospheric turbulence," *J. Opt. Soc. Am.* **69**, 73–84 (1979).
7. S. C. H. Wang and M. A. Plonus, "Optical beam propagation for a partially coherent source in the turbulent atmosphere," *J. Opt. Soc. Am.* **69**, 1297–1304 (1979).
8. L. Fante "Intensity fluctuations of an optical wave in a turbulent medium, effect of source coherence," *Opt. Acta* **28**, 1203–1207 (1981).
9. T. Friberg and R. L. Sudol, "Propagation parameters of Gaussian Schell-model beams," *Opt. Comm.* **41**, 383–387 (1982).
10. V. A. Banakh, V. M. Buldakov, and V. L. Mironov, "Intensity fluctuations of a partially coherent light beam in a turbulent atmosphere," *Opt. Spektrosk.* **54**, 1054–1059 (1983).
11. Y. Baykal, M. A. Plonus, and S. J. Wang, "The scintillations for weak atmospheric turbulence using a partially coherent source," *Radio Science* **18**, 551–556 (1983).
12. Y. Baykal and M. A. Plonus, "Intensity fluctuations due to a spatially partially coherent source in atmospheric turbulence as predicted by Rytov's method," *J. Opt. Soc. Am. A* **2**, 2124–2132 (1985).
13. T. Yoshimura, "Statistical properties of dynamic speckles," *J. Opt. Soc. Am. A* **3**, 1032–1054 (1986).
14. H. T. Yura, S. G. Hanson, and T. P. Grum, "Speckle statistics and interferometric decorrelation effects in complex ABCD optical systems," *J. Opt. Soc. Am. A* **10**, 316–323 (1993).
15. H. T. Yura, S. G. Hanson, and L. Lading, "Laser Doppler velocimetry: analytical solution to the optical system including the effects of partial coherence of the target," *J. Opt. Soc. Am. A* **12**, 2040–2047 (1995).
16. J. C. Ricklin and F. M. Davidson, "Atmospheric turbulence effects on a partially coherent Gaussian Beam: implications for free-space laser communication," *J. Opt. Soc. Am. A* **19**, 1794–1802 (2002).
17. J. C. Ricklin and F. M. Davidson, "Atmospheric optical communication with a Gaussian Schell beam," *J. Opt. Soc. Am. A* **20**, 856–866 (2003).

18. L. Mandel and E.Wolf, *Optical Coherence and Quantum Optics* (Cambridge University Press, Cambridge, 1995).
19. A. C. Schell, "The Multiple Plate Antenna" (Doctoral Dissertation, Massachusetts Institute of Technology, Cambridge, Mass., 1961).
20. V. A. Banakh and V. M. Buldakov, "Effect of the initial degree of spatial coherence of a light beam on intensity fluctuations in a turbulent atmosphere," *Opt. Spectrosk.* **55**, 707–712 (1983).
21. O. Korotkova and L. C. Andrews, "Speckle propagation through atmospheric turbulence: effects of a random phase screen at the source," Proc. SPIE **4821**, 98–109 (2002).
22. O. Korotkova and L. C. Andrews, "Speckle propagation through atmospheric turbulence: effects of partial coherence of the target," Proc. SPIE **4723**, 73–84 (2002).
23. O. Korotkova, L. C. Andrews, and R. L. Phillips, "A model for a partially coherent Gaussian beam in atmospheric turbulence with application in lasercom," *Opt. Eng.* **43**, 330–341 (2004).
24. O. Korotkova, L. C. Andrews, and R. L. Phillips, "The effect of partially coherent quasi-monochromatic Gaussian-beam on the probability of fade," Proc. SPIE **5160**, 68–77 (2003).
25. P. Beckmann and A. Spizzichino, *The Scattering of Electromagnetic Waves from Rough Surfaces* (Pergamon, New York, 1963).
26. J. A. Olgilvy, *Theory of Wave Scattering from Random Rough Surfaces* (Adam Hilger, Bristol, 1991).
27. J. W. Goodman, *Statistical Optics* (Wiley, New York, 1985).
28. A. Dabas, P. H. Flamant, and P. Salamitou, "Characterization of pulsed coherent Doppler lidar with speckle effect," *Appl Opt.* **33**, 6524–6532 (1994).
29. P. Drobinski, A. M. Dabas, P. Delville, P. H. Flamant, J. Peron, and R. M. Hardesty, "Reflective-index structure parameter in the planetary boundary layer: comparison of measurements taken with a 10.6-μm coherent lidar, a 0.9-μm scintillometer, and *in situ* sensors," *Appl Opt.* **38**, 1648–1656 (1999).
30. O. Korotkova, L. C. Andrews, and R. L. Phillips, "A lidar model for a rough-surface target: method of partial coherence," Proc. SPIE **5237**, 49–60 (2003).